Materials Today Sustainability 24 (2023) 100517

Contents lists available at ScienceDirect

Materials Today Sustainability

journal homepage: https://www.journals.elsevier.com/materials-today-sustainability

Investigation of CO_2 sequestration performance and statistical analysis of dye removal efficiency of liquefied hornbeam based carbon foams: Effects of biomass/solvent weight ratio, tar contribution, and chemical activation

A.S. Yargic*, G. Gunduz Meric, R.Z. Yarbay, N. Ozbay

Chemical Engineering Department, Engineering Faculty, Gulumbe Campus, Bilecik Seyh Edebali University, 11100, Bilecik, Turkey

ARTICLE INFO

Article history:
Received 17 May 2023
Received in revised form
9 August 2023
Accepted 22 August 2023
Available online 25 August 2023

Keywords:
Analysis of variance
Carbon foam
CO_2 and dye uptake
Hornbeam sawdust
Solvolytic liquefaction

ABSTRACT

The preparation of carbon foams from bio-based polyols was a preferable alternative for the development of new materials from waste resources. The research described the usage of wood processing factory waste for the production of open-cell carbon foams with a high application potential. Bio-based carbon foams were developed by hornbeam tree sawdust, a low-cost and renewable material for dye removal via adsorption and CO_2 uptake performance. In this work, the influences of the solvent type, and solvent/biomass weight ratio on the characteristics of carbon foams were investigated in the solvolytic liquefaction process. A chemical activation process with KOH was applied to the foams and this provided high porosity and surface area (up to 1454 m^2/g). Carbon foams were found to have comparable compressive strengths; up to 1.080 MPa. As a result of the statistical analysis, according to the variance analysis performed with a confidence level limit of 95%, it was specified that pH had a negative coefficient and was the most significant factor in *NH* dye removal. According to the experiments carried out within the scope of investigating the usability of carbon foams in the removal of pollutants from gas and liquid systems, *HCFTA-3* carbon foam exhibited a maximum removal efficiency of 55.2% for *NH* dye when pH was 2, and *HCFA-3* carbon foam had the highest CO_2 holding capacity at 0 °C as measured by 6.53 mmol/g CO_2. This study provided an understanding of the sustainable bio-based carbon foams from industrial waste biomass for practical application of green chemistry.

1. Introduction

The carbon foams have taken attention according to their tunable 3D porous structure, which can be controlled by choosing suitable raw materials and preparation methods and outstanding performance in many application areas [1,2]. To develop more competitive carbon materials, consideration should be given to evaluating the usage of renewable resources as an alternative to fossil fuel-derived pitches or phenolic resin from the reaction of phenols and aldehydes. Biomass, the only renewable carbon source that includes animal/agricultural products and wastes [3], has recently attracted significant attention as an alternative and essential source due to its striking features, for instance, low sulfur and nitrogen content, environmental friendliness, and carbon neutrality [4]. The low density, controllable thermal conductivity, high-temperature resistance, flame retardancy, and mechanical strength of carbon foams enable their usage as a core in sandwich hybrid systems for aerospace and shipbuilding implementations. The carbon foams can be utilized efficiently in several applications, such as electrodes, energy storage systems, oil spill remediation systems, electromagnetic interference shielding materials, catalytic supports, and adsorbents [2]. Consequently, CO_2 and dye adsorption have become a particular focus of contemporary research in this work.

The increase in the concentration of CO_2 from fossil fuel combustion and many further anthropogenic activities has turned into the most substantial concern of global warming and climate change. The world energy outlook estimates that CO_2 emissions from fuel-burning emissions will be enlarged to 40.2 Gigatons of CO_2 by 2030 [5]. Therefore, the utilization of CO_2 adsorption in the

* Corresponding author.
E-mail address: seyda.guler@bilecik.edu.tr (A.S. Yargic).

https://doi.org/10.1016/j.mtsust.2023.100517
2589-2347/

areas of energy and the environment has been remarkably extensive. Applications include CO_2 reduction, fuel synthesis using CO_2, and CO_2 separation from contaminated gases. The issues to be resolved during the CO_2 capture and activation process can be listed as the strength of the C–O bond in CO_2 and the adsorption energy between CO_2 and substrate [6]. The adsorption method involving solid materials for CO_2 capture was suitable due to its low energy demand, high viability for scale-up operations, moderate processing conditions, simple regeneration, and lack of contaminants or byproducts [7]. Various solid adsorbents including, zeolite [8], mesoporous silica [9], MOFs (metal-organic frameworks) [10], and activated carbon have been evaluated. While the microporous structure rather than the mesoporous structure is more practical for CO_2 capture, silica primarily contains a significant quantity of mesoporous structure [11]. While zeolite and MOFs have some limitations like high cost and decreasing adsorption capacity under humid conditions as a result of their hydrophilic nature, other materials like porous carbon that shows noticeable CO_2 sorption capacity at 1 bar and 25 °C have gained interest due to its advantages of having a wide range of raw material sources, simple formation, superior mechanical and thermal stability, hydrophobicity, reduced regeneration energy demand, and handy surface chemical/porosity modifiability [12].

Another research interest of this study is dye adsorption. Zeolites, mesoporous silicas, MOFs (metal-organic frameworks), and activated carbons were only a few of the many adsorbents that are employed for dye removal. Among these materials used, carbon-based materials showed high removal efficiency, which made them the center of interest. Priyanka and Saravanakumar [13] studied the production of zinc-based carbon foam-like structures (Zn-CFst) from starch for the adsorption of hazardous dyes and the separation of oil from water. Zn-CFst material displayed extremely high adsorption capacities for Congo Red (1428.57 mg/g), Malachite Green (1200 mg/g), and Crystal Violet (25000 mg/g) dyes, as well as high capacities for Castrol 2T (2937%) and Gear oil (2375%). Zhang et al. [14] prepared carbon foam with adjustable pore size distribution by a one-pot lava foam process to utilize in Malachite Green removal. They reported that even though carbon foams pore size distribution was shown to be a dominating component in dye removal, the maximum adsorption capacity was as high as 1812 mg/g. In a different work, phenolic resin-containing iron acetylacetonate was in-situ pyrolyzed to produce magnetic carbon foam, which was then applied as an adsorbent to remove the dye Rhodamine B [15]. Their findings highlighted the fact that the adsorption equilibrium was attained in 40 min and that the highest adsorption capacity was 258.03 mg/g. For the elimination of Methylene Blue, Li et al. [16] investigated pitch-based carbon foam produced by applying the self-foaming technique with mesophase pitch as the precursor. They concluded that the adsorption rate and capacity of composites were enhanced by 158.18% and 93.50%, respectively, when compared to raw carbon foam. Lu et al. [17] prepared carbonized TiO_2-coated melamine foam (CTiMF) via polydopamine and used it in the photocatalytic degradation of Rhodamine B. They stated that the crucial role of the carbonization process was improving the anchoring stability of TiO_2 on the melamine foam. Moreover, they highlighted that the CTiMF showed excellent photocatalytic activity for Rhodamine B decomposition under artificial sunlight irradiation recording as 16 times higher than TiMF.

The development of carbon foam utilizing biomass as an alternative to carbon foams made from mesophase pitch or phenol-aldehyde resins was the primary objective of this research. Within the scope of the study, considering that carbon foams can be used as an adsorbent in gas and liquid systems, it has been studied on the evaluation of carbon foams produced by solvolytic liquefaction of biomass and resinification of the bio-polyol as adsorbent. In addition, the adsorption performance of the tar-added carbon foams produced within the scope of examining the usability of the pyrolysis liquid product as a solvent in the solvolytic liquefaction procedure was also investigated.

2. Materials and methods

2.1. Raw material and pyrolysis tar

A wood processing facility in Eskişehir (Turkey) provided the waste sawdust of hornbeam trees (*HS*), which was subsequently air-dried in the lab to develop carbon foam. In the first step, a grinder (Armfield FT-7A) was used to minimize the raw materials particle size, the average particle size and the bulk density were calculated as 0.497 mm and 0.26 g/cm^3, respectively. Moisture, ash, volatile matter, fixed carbon, extractive material, holocellulose, lignin, hemicellulose, and cellulose contents were determined by performing preliminary and structural analysis of *HS*. The thermal behavior of *HS* in the temperature range of 20–1000 °C was analyzed by TG analyzer (Setaram Labsys Evo), and the ultimate analysis was carried out via Elemental Analyzer (Leco CNH628 S628) to determine CHN contents at 950 °C. Functional groups of *HS* were specified by the attenuated total reflectance-Fourier transform infrared (ATR-FTIR) spectroscopy (Perkin Elmer Spectrum 100) in the range of 4000–400 cm^{-1} with a resolution of 4 cm^{-1} after 100 scans. The sample was platinum-coated by Quorum Q 150 R ES DC Sputter to clarify the surface morphology through a scanning electron microscope (SEM, Zeiss Supra VP 40).

In the slow pyrolysis experiments carried out in the Heinze reactor at 400 °C under a static environment, the heating rate was set to 10 °C/min and the reaction time to 20 min. Our related papers provide a detailed description of the experimental procedure [18–20]. The gaseous, liquid, and solid pyrolysis product yields determined on a dry ash-free basis were 22.37%, 19.95%, and 30.32%, respectively. Characterization results of the structure of pyrolysis tar ($HS_{@400°C}$) elucidated using Fourier transform infrared spectroscopy (FT-IR, Perkin Elmer Spectrum 100), nuclear magnetic resonance spectroscopy (^{1}H NMR, Varian Mercury 300 MHz), gas chromatography/mass spectroscopy (GC/MS, Shimadzu GC-2010 Plus), and elemental analyzer (Leco CHN628, S628) were given in the previous study [18].

2.2. Synthesis and characterization of HS-based carbon foams

For the production of carbon foam by solvolytic liquefaction of *HS* with a particle size of $0.25<d_p<0.85$ mm, the syntheses were carried out in two different solvent mediums (phenol or phenol + tar mixture) [19,21]. Carbonaceous materials containing graphene-like structures were prepared by using phenol (Merck) as a solvent in the liquefaction process to generate conventional phenolic resins in the first stage. In the second step, the usability of the "phenol + tar" mixture as an alternative solvent to phenol was investigated. In the carbon foam production by using tar, the same traditional phenolic resin production method was applied, and the phenol proportion added in the liquefaction stage was changed by tar at a 40-wt percent rate. The effects of solvent type, solvent/biomass weight ratio (3/1 or 5/1 w/w), and chemical activation with potassium hydroxide on foam properties were examined by various characterization techniques. Bio-polyol formed after mixing *HS* (10 g) and solvent (30 g or 50 g "phenol" or "60 wt% phenol+40 wt% tar mixture") under reflux for 1 h at a temperature range of 124–136 °C in an acidic medium containing a mixture of sulfuric acid (98 wt%, Merck) and phosphoric acid (85 wt%, Panreac), separated from the residue using the solvent methanol. After adjusting the pH of the solution to neutral with sodium carbonate (anhydrous, Panreac) and removing the solvent from the medium,

liquefied-*HS* was obtained. Formaldehyde (37 wt%, Merck), sodium hydroxide (analytical grade, ADR), and distilled water were added to it, and the reaction was carried out first at 55–60 °C for 2 h, then at 95–98 °C for 1 h, respectively. The pH of the cooled mixture was adjusted to be neutral, polysorbate-80 (Merck), n-pentane (Merck), and sulfuric acid were added to the resin obtained by removing the water phase, and *HS*-based resin foam (coded as *HRF* and *HRFT*) was produced by placing the mixture into the mold and heating it at 60 °C for 24 h. Carbon foam was prepared by carbonizing the resin foam at 800 °C for 2 h under a nitrogen environment. The foaming agent (n-pentane), which must be transferred away from the resin medium during the foaming stage and form a porous foam structure, was unable to overcome the surface tension due to the tar structure so rigid and less porous foams were produced when tar was combined with phenol. The porosity was enhanced by increasing the surfactant proportion in the synthesis recipe by 25% during the foaming stage of the processes in which tar was added to synthesize the carbon foams developed for application in the adsorption process.

The activation process was applied using potassium hydroxide (KOH) with a ratio of resin foam/chemical agent to 1/1 by weight to enhance the surface area of the resin foams. In the first step of this method, the resin foam was mixed with the KOH solution at 100 °C, and the moisture was removed in an oven. In the second step of preparing activated-carbon foam, the foam treated with KOH was first carbonized at 800 °C in a tube furnace, then washed with hot distilled water and dried until no K^+ ions remained in the structure. Carbonized and activated foams were labeled as *HCF-x* and *HCFA-x*. Where, *-x* denotes the solvent ratio, coded as *-3* or *-5* for solvent/biomass weight ratio of 3/1 or 5/1 w/w, respectively. The solvent kind was also denoted as *-T* for the phenol + tar mixture.

Thermogravimetric analysis (Setaram Labsys Evo) was used to assess the thermal stability of resin foams. The thermogravimetric analysis technique involved heating the resin foams from room temperature to 800 °C at a rate of 20 °C/min under an argon environment. Elemental analysis (Leco CHN628, S628) was carried out to examine the CHN compositions of the carbon foams. Fourier transform infrared spectrums in the wavelength range of 4000–400 cm^{-1} were taken using Agilent Cary 630 device to identify the functional groups in the carbon foams structures. The surface morphologies (particle sizes, shapes, and distributions) and textures of the foams were analyzed by the scanning electron microscope (Zeiss Supra VP 40) and the transmission electron microscope (Jeol 1220 JEM, 80 keV). The determination of crystal structures of the foams and the calculation of the interlayer spacing (d-spacing) values in the atomic lattice were assigned using an x-ray diffraction device (PANalytical Empyrean) and CuKα radiation (λ = 0.15406 nm). X-ray diffraction patterns were acquired in the 2θ range of 0° and 80° at a scan rate of 2°/min. BET surface areas (S_{BET}), pore volumes, and pore size distributions of the foams were established via the Micromeritics ASAP 2020 device handling nitrogen as an adsorptive at 77 K. Confocal Raman spectra of the foams were acquired via the RENISHAW Raman inVia microscope. The foams compressive strengths were measured in a Shimadzu AG-IC 100 KN tensile/compression device with a 0.5 mm/min loading rate, and the true densities were specified with a helium gas pycnometer (Micromeritics, Accupyc II 1340). In addition, the bulk densities and the %porosity values were calculated. To quantify the porosity(%), the formula in Eq. (1) was taken into account. Where, the value of P, V_t, and V_a is defined as %porosity, the theoretical and actual volume of foam [22].

$$P = (V_t - V_a) / V_t \quad (1)$$

2.3. Dye removal via adsorption and CO_2 uptake performance

Within the scope of the research, it was aimed to evaluate carbon foams as adsorbents for gas and liquid systems. In order to complete the step of examining the usability of carbon foams in systems containing gas phase impurities, which was one of the main objectives of the study, the CO_2 holding capacities of adsorbents were determined. Furthermore, the efficacy of hornbeam-based carbon foams in the elimination of *Procion Navy H-EXL* dye, supplied by DyStar, from aqueous solutions was examined. Neither any purifying procedures were used before dissolving the reactive textile dye *Pr Navy H-EXL* (*NH*, reactive blue) with a double monochlorotriazine reactive group and chromophore azo [23]. Distilled water was used to prevent and reduce any contaminants while preparing dye solutions, and dissolving 1.0 g of *NH* dye in 1000 mL of distilled water yielded a standard dye solution (1000 ppm). A solution with a dye concentration of 25 mg/L was created by diluting the stock dye solution. To change the solution pH, 0.1 M NaOH or 0.1 M HCl was added, and the Thermo Scientific Orion 3 Star digital pH meter was used to measure the result. The effects of variables on *NH* dye uptake, including pH, solvent/biomass weight ratio, solvent type (tar integration), and chemical activation, were examined by batch sorption studies in a group of conical test tubes comprising 50 mL of *NH* solution. The carbon foams with a sorbent dosage of 2 g/L added to the dye solution were shaken for 75 min in a water bath at room temperature for the adsorption experiments. After filtration of the suspensions, calibration curves were created to determine the amount of dye in the filtrate, and concentration values were acquired by measuring absorbance at λ_{max} = 607 nm for *NH* dye with a UV/visible spectrophotometer (Agilent Cary 60 UV–Visible Spectrophotometer). In Eq. (2), which was used to calculate the dye removal efficiency (η) from aqueous solutions, the terms C_0 and C_e (mg/L) were defined for the initial and equilibrium dye concentrations in the liquid phase [24]:

$$\eta\ (\%) = [(C_0 - C_e) / C_0]\ 100 \quad (2)$$

2.4. Statistical modeling of dye adsorption with full factorial experimental design

It is possible to reduce the overall number of trials, time, and research costs by using a factorial experimental design; besides optimization of the process can be realized by estimating the effects of all the main factors and the interaction effects of the factors correctly. In the full factorial experimental design method, the relationship between all factors can be assessed depending on the number of levels determined. In this study, $2^4 = 16$ dye adsorption experiments were carried out in a two-level full factorial experimental design of 4 factors (the effects of solvent/biomass weight ratio of 3/1 and 5/1, tar contribution (0% and 40%), chemical activation (applied and not applied), and pH of 2 and 8). The main factors were symbolized by a low level of "-1" and a high level of "+1" in statistical charts, as given in Table 1.

Table 1
The main factors levels involved in 2^4 full factorial design of *NH* dye sorption.

Factors	Levels	
	Low level	High level
Solvent/biomass weight ratio (*A*)	−1	+1
Tar contribution (*B*)	−1	+1
Chemical activation (*C*)	−1	+1
pH (*D*)	−1	+1

3. Results and discussion

3.1. Summary of essential properties of HS and $HS_{@400^{\circ}C}$

Hornbeam sawdust's high volatile (85.21%) and low ash (0.45%) contents make *HS* favorable for tar production. The fact that hornbeam sawdust had a considerable lignin content of 30.92% was an indication that the phenolic compounds in its structure were high. The elemental carbon (45.99%) and lignin (30.92 wt%) contents of *HS* were prominent to get tar and carbon foam. Following the results of the elemental analysis and using Dulong's equation, the calorific value of *HS* was also computed to be 16.33 MJ/kg [25]. According to the SEM image (taken at 5000x magnification), *HS* had a non-porous fibrous morphology. In our earlier work, the findings from the analysis of the biomass feedstock were thoroughly discussed [18].

It was established that the calorific value (24.82 MJ/kg) and carbon content (59.94%) of tar were higher than those of raw material. Compared to cellulose, hemicellulose, and lignin in the feedstock, the tar contained organic compounds with different structures. According to the chemical shift values of various hydrogen atoms specified from the spectrum obtained from the ^{1}H NMR analysis, lignocellulosic biomass-based tar had an aromatic fraction of 16.45% due to the presence of phenolic compounds. The tars of lignocellulosic-based raw materials contain similar compounds such as phenolic compounds, aldehydes, ketones, and carboxylic acids. In the GC/MS chromatogram of $HS_{@400^{\circ}C}$, it was identified that the prominent peaks (with areas greater than 10%) including phenol; 2-methyl-phenol; 2-ethyl-phenol; 3-ethyl-phenol; 2,4-dimethyl-phenol; 4-methyl-phenol; 4-propyl-phenol; 3-ethyl-5-methyl-phenol; 3,4,5-trimethyl-phenol belonged to phenolic compounds. Furfural and furan compounds were also detected.

3.2. Characterization of foams

3.2.1. Thermogravimetric analysis of resin foams

In Fig. 1, the TG and dTG graphs demonstrate the influence of different solvents and solvent/biomass weight ratios on the thermal degradation properties of liquefied hornbeam sawdust-based resin foams. Table 2 depicted the amount of residual carbon still present after weight losses and temperature values for different degradation phases. It was revealed from the TG and dTG profiles of the *HS*-based resin foams that the materials were decomposed during heat treatment in two phases. Weight loss resulted in the first phase between 30 and 320 °C as a result of the elimination of remaining moisture and low-molecular-weight molecules (curing/foaming additives, unreacted phenol-formaldehyde). The deformation of intermolecular ether bonds and terminal hydroxymethyl groups, the bond breaks at various locations throughout the main chain of the phenolic resin, and the discharge of volatile compounds all contributed to weight reduction in the second phase [19,21,26,27]. The formation of phenols and cresols was clarified in studies investigating the thermal degradation of phenol-formaldehyde resin due to the scission of a terminal benzene ring depending on the location of the scission [28], and it was also pointed out that there was a potential of xylenol or trimethyl phenol formation [29,30]. Jiang et al. [31] reported that methylene in the structure of phenol-formaldehyde resin was active, and its breakdown was the primary factor in the pyrolysis of the phenol-formaldehyde resin. Accordingly, methylene and the phenolic hydroxyl were further cross-linked initially, then some methylene molecules were scissored, resulting in the production of volatiles that contain phenol and its methyl derivatives. It was underlined that the general decomposition takes place in the temperature

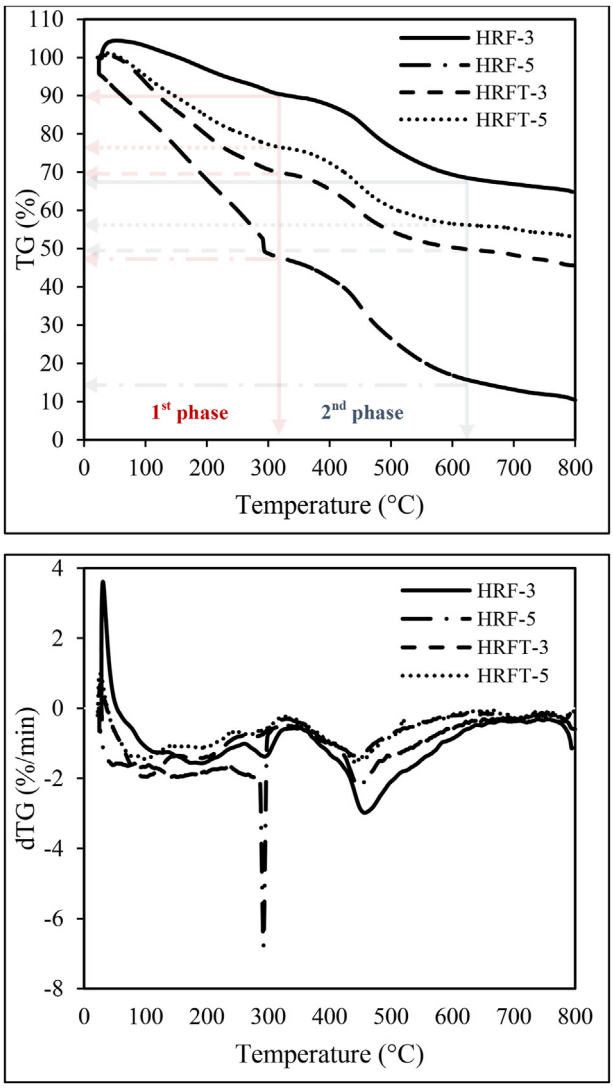

Fig. 1. TG and dTG curves for *HS*-based resin foams.

Table 2
Thermal decomposition parameters of resin foams.

Foam code	1st degradation step		2nd degradation step	
	T_D (°C)[a]	C_R (%)[b]	T_D (°C)[a]	C_R (%)[b]
HRF-3	30–320	90.38	320–620	68.62
HRF-5	30–320	47.61	320–620	15.87
HRFT-3	30–320	69.89	320–620	45.56
HRFT-5	30–320	76.49	320–620	53.20

[a] T_D: The degradation temperature.
[b] C_R: Residual carbon after degradation.

range of 400–600 °C in the fundamental study that investigated the thermal degradation of phenol-formaldehyde polycondensates [32]. Carbon monoxide, carbon dioxide, benzaldehyde, benzene, and toluene are generated by thermal oxidative processes, whereas methane, phenol, and phenolic homologs are formed by thermal decomposition reactions. The peak intensity attributed to ether bonds at 1110 cm^{-1} decreased as a result of ether bond cleaving, as evidenced by the FT-IR study results. While certain studies have associated this peak with aromatic in-plane CH vibration, other scholars have proposed that it may be caused by ether-type links, ether-type linkages, or a combination of both contributions. Owing

to the existence of phenolic and non-phenolic dimers, the breakdown of ether bonds was reported to take place between 200 °C and 400 °C in temperature ranges. In phenolic substances, the α-ether bond's heterolysis breakage can yield a quinone methide intermediate, which may contribute to the β-ether bond's simultaneous homolytic cleavage at 200 °C [33]. The quick weight loss in the range of up to 320 °C for *HRF-5* was caused by the structural decomposition as a result of the fact that phenol, which was introduced to the synthesis medium more, promoted self-combustion due to the oxygen in its structure, therefore it was revealed that *HRF*-5 had inferior thermal stability than *HRF-3*. It was found that the percentage of residual carbon declined from 68.62% to 15.87% when more phenol was incorporated into the reaction mixture. By evaluating dTG curves, it was concluded that resin foams degraded noticeably quickly between 320 and 620 °C. When the amount of solvent was raised or tar was added, it was noticed that the initial decomposition temperature reduced somewhat in comparison to the conventional methods solvent/biomass weight ratio of 3/1. The early degradation of the chemical agents existing in the resin foams could be responsible for the slight drop in the primary decomposition temperature of the resin foams. The DTG curves most significant endothermic peaks were detected at about 300 °C and between 440 and 465 °C. It was obvious that when tar was incorporated into phenol as a solvent, the hydroxyl and methoxyl groups of the guaiacyl and syringyl units that compose the tar, in addition to the hydroxyl group in the structure of the phenol, caused oxidative decomposition of the resin foams depending on the heating process employed in the thermogravimetric analysis. Using phenol and tar-mixed phenol as solvents, we systematically reported the phenolization, polymerization, and condensation reaction mechanisms that occurred during the solvolytically liquefaction of the woody structure and the production of phenol-formaldehyde resin [19].

3.2.2. FT-IR analysis

FT-IR spectrums in which the functional groups in the carbon foams structure were examined and presented in Figs. 2 and 3 depending on the solvent type/ratio and chemical activation process. It was specified that the FT-IR spectrums of the carbon foams were almost similar; it was concluded that the differences in the structure were negligible by changing the solvent type or solvent ratio in the production methodology and the application of the chemical activation. The presence of C≡CH alkyne stretching vibrations in the FT-IR spectrums was demonstrated by the peak observed around 2100 cm^{-1}. The peaks of unconjugated C=O (aldehyde, ketone, carboxylic acid) stretching vibration were close to 1700 cm^{-1}, the stretching band of $C=C_{ar}$ indicating the presence of aromatic structures was in the range of 1600–1400 cm^{-1}, the bending band of CH for guaiacyl and syringyl derivatives was around 1115 cm^{-1}, and the peaks of substituents attached to the aromatic ring were observed in the band range of 900–700 cm^{-1} [34–36]. It was noticed from the peaks in the spectrum that neither the solvent type/ratio nor chemical activation significantly shifted the peaks, and all carbon foams T% values were quite close to one another. On the other hand, adding tar to phenol as a solvent during the synthesis of carbon foam slightly reduced the peak intensity and raised T% values without the chemical activation (Figs. 2a-b and 3a-b). The peaks at 1100 cm^{-1} were seen to vanish after the chemical activation. Instead of the CH bending band at 1110 cm^{-1}, the $C=C_{ar}$ stretching band at 1500 cm^{-1} became more evident as the solvent ratio increased, suggesting the existence of aromatic structures.

3.2.3. Elemental analysis

The C, H, O, and N components of carbon foams were analyzed by elemental analysis, and the results were given in Table 3. The changes in carbon content, H/C, and O/C ratios in the structure were compared depending on the solvent/biomass ratio, solvent type, and chemical activation process. The carbon contents of the foams were greater than those of the raw material (45.99% C) and tar (59.94% C), revealing that they were more carbon-containing materials than *HS*. When only phenol was used as the solvent for the phenol/biomass ratio of 3/1, the carbon content and the calorific value of the foam were determined as 80.8% and 32.47 MJ/kg,

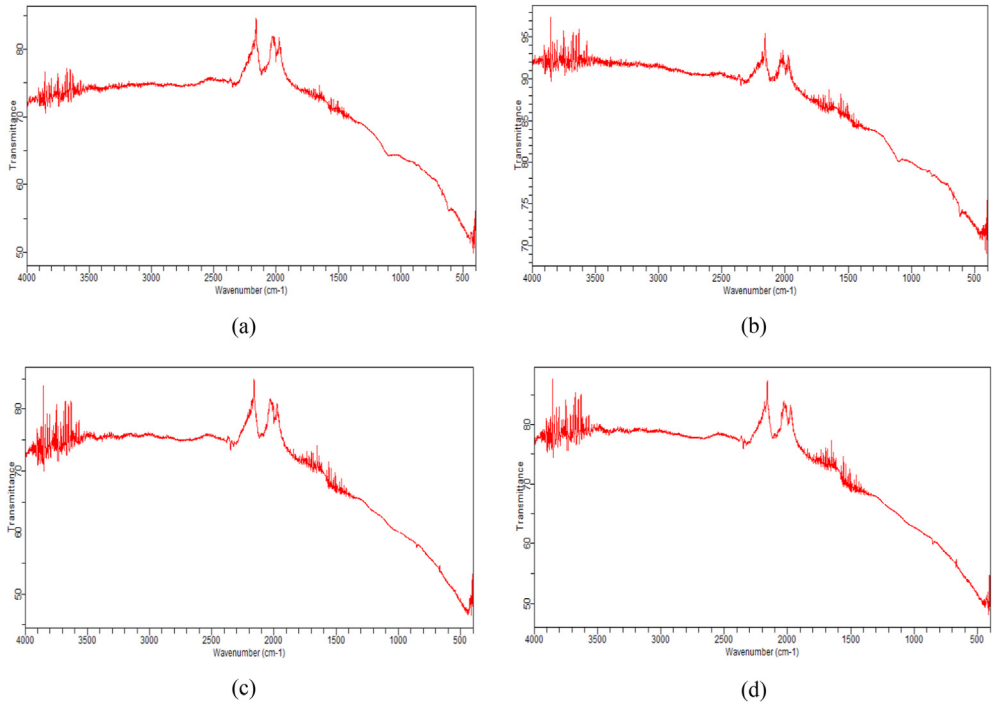

Fig. 2. FT-IR spectrums of carbon foams for solvent/biomass weight ratio of 3/1; (a) *HCF-3*, (b) *HCFT-3*, (c) *HCFA-3* and (d) *HCFTA-3*.

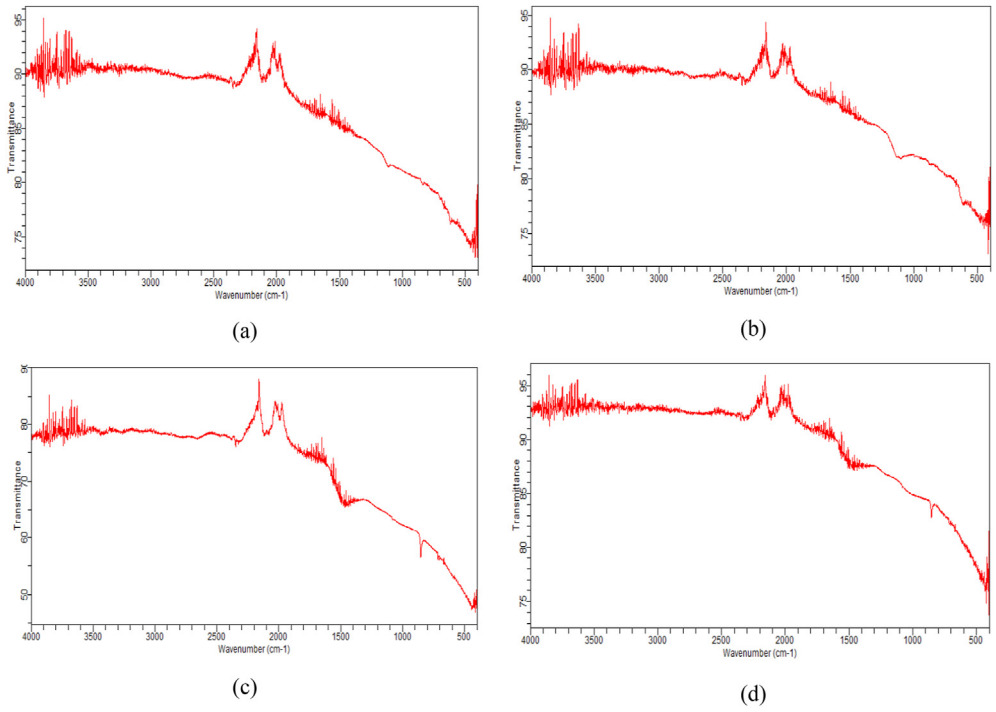

Fig. 3. FT-IR spectrums of carbon foams for solvent/biomass weight ratio of 5/1; (a) *HCF-5*, (b) *HCFT-5*, (c) *HCFA-5* and (d) *HCFTA-5*.

Table 3
Elemental analysis results of carbon foams produced by solvolytic liquefaction of *HS*.

S/B ratio	Foam code	C (%)	H (%)	O (%)	N (%)	HHV (MJ/kg)	H/C	O/C
3/1	*HCF-3*	80.811	5.106	12.332	1.751	32.473	0.76	0.11
	HCFT-3	80.723	3.028	15.220	1.029	28.924	0.45	0.14
	HCFA-3	60.741	5.322	33.636	0.301	22.155	1.05	0.42
	HCFTA-3	60.946	3.791	35.027	0.236	19.764	0.75	0.43
5/1	*HCF-5*	77.134	4.604	17.743	0.519	29.529	0.72	0.17
	HCFT-5	80.985	3.108	14.680	1.227	29.226	0.46	0.14
	HCFA-5	60.071	3.632	36.066	0.231	19.052	0.73	0.45
	HCFTA-5	59.789	3.8994	36.099	0.213	19.336	0.78	0.45

respectively. It was found that when the phenol quantity integrated into the reaction mixture increased, the carbon content of the foam decreased to ~77%, and the calorific value decreased to 29.53 MJ/kg. Furthermore, when the phenol + tar mixture was added to the synthesis medium as a solvent, the carbon content and the calorific value of the foams changed between 80.723 and 80.985% and 28.924–29.226 MJ/kg, respectively. After the chemical activation process was applied, it was observed that the carbon content and the calorific value of the foams reduced by 22–26% and 31–35%, respectively. The high oxygen content of tar (28.53%) and the participation of methoxy, carbonyl, and hydroxy groups in the tars structure resulted in an increase in the carbon foams O/C ratios when tar was used during the synthesis of carbon foam [18,37].

3.2.4. Structural analysis

Carbon foams nitrogen adsorption/desorption isotherms were displayed in Figs. 4 and 5. It was specified that carbon foams had type-IV isotherms belonging to solid materials containing mesopores and micropores in their structures as seen in Figs. 4 and 5. The slow increase of isotherms at $P/P_0 < 0.1$ relative pressure showed that the carbon foams had micropores in this region. According to the isotherms, an increase in the adsorbed volume was observed in the range of $0.01 < P/P_0 < 0.30$. This situation proved that there was a regular distribution of mesopores in the structures. The increase in the adsorbed volume after the $P/P_0 > 0.9$ indicated that there was macroporosity in the structure of the foams. In general, the hysteresis region formed in the adsorption and desorption isotherms identifies that the pore shapes in the structure of carbon foams are not homogeneous. It was agreed that the carbon foams synthesized by adding tar showed parallel trends to the nitrogen adsorption/desorption isotherms of the carbon foams prepared by the conventional process. Numerous activated carbons and a few other nanoporous adsorbents exhibit type H4 loops. In the simplest scenario designed for these isotherms, multilayer physisorption, and capillary condensation follow the first region of reversible micropore filling [38]. As seen in Figs. 4 and 5, the nitrogen isotherms exhibited type H4 hysteresis loops, which clarifies the nature of carbon foams narrow slit-like pores. It is well known that until P/P_0 values are quite near the saturation pressure, the H4 hysteresis loop shape typically does not close [39].

Nitrogen adsorption parameters of carbon foams were presented in Table 4. Surface area (Brunauer, Emmett and Teller method-S_{BET}) values were obtained as 467.492 m^2/g and 472.130 m^2/g for *HCF-3* and *HCF-5*, respectively. Accordingly, when the amount of phenol added to the liquefaction process increased, it was seen that the surface area of the carbon foam was improved. However, as the tar was evaluated as a solvent in the solvolytic liquefaction reaction as well as phenol, it was noticed that the

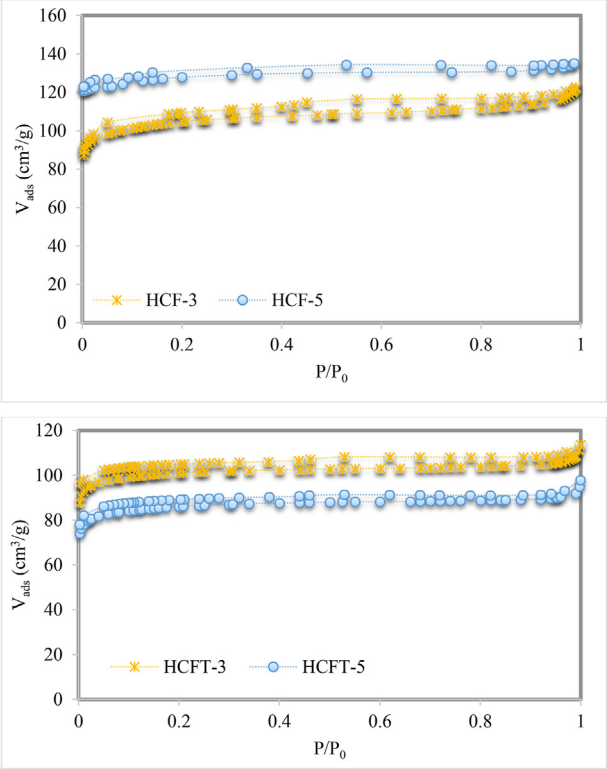

Fig. 4. Adsorption/desorption isotherms of carbon foams (effect of solvent type and ratio).

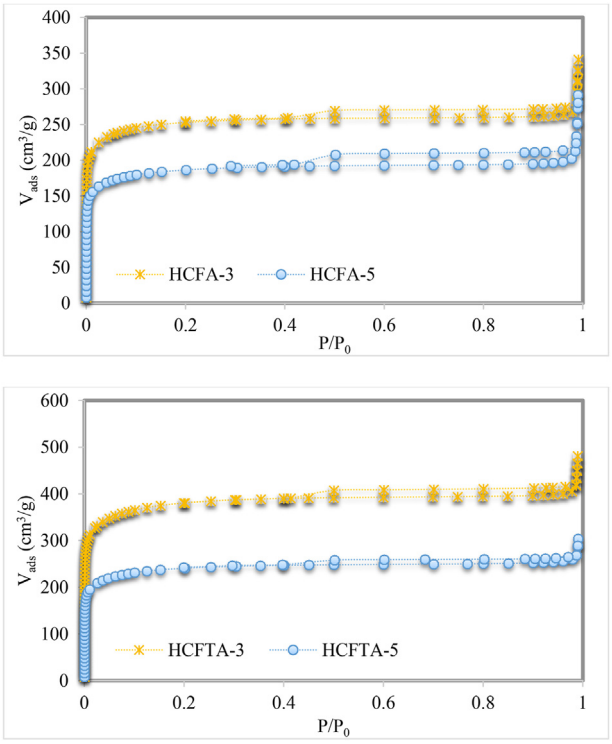

Fig. 5. Adsorption/desorption isotherms of carbon foams (effect of chemical activation).

surface area declined by ~48% and 34% when compared to the same solvent/biomass ratio. In the liquefaction process where tar was used as a solvent additive, the amount of tar in the structure increased with the augment in the solvent proportion, causing carbon foams with lower surface area to be obtained. Because of the complicated composition of the tar, more rigid polymeric materials were formed when tar was used during the synthesis step instead of phenol. As a result, it was difficult to remove the reaction mixtures foaming chemicals from the polymer matrix. Due to the raise in the polymer matrix surface tension, the gas molecules could not leave the synthesis medium, which prevents the occurrence of pores on the surface [19]. After the chemical activation process, the increase in the surface area and pore volume values was remarkable. It was ascertained that the surface area values of carbon foams, which were prepared using tar and activated with KOH, increased by 1.98–4.98 times. Carbon foam synthesized and activated with KOH when the solvent/biomass ratio is 5/1 had the highest surface area and total pore volume of 1454.39 m^2/g and 0.62308 cm^3/g. The distribution of pore sizes is an important factor in the microstructural characterization of carbon foams. In addition, according to the average pore diameter (D_{av}, nm) values (Table 4) and the pore size distribution graphs (Figs. 6 and 7), the foams had mesoporous structures (D_{av} > 2 nm). When the phenol/biomass weight ratio changed from 3/1 to 5/1, the reduction in average pore size was closely related to the increase in surface area. In summary, the surface areas of the foams produced by the liquefaction technique were 243.231–1454.39 m^2/g, the total pore volumes were 0.1593–0.6231 cm^3/g, and the average pore diameter values were in the range of 12.03–2.76 nm. In the literature, the structural properties of carbon foams obtained as a result of the solvolytic liquefaction of larch, birch, oak, and spruce sawdust have been investigated. Accordingly, the surface areas of the foams produced by the liquefaction method are 209–1918 m^2/g, the total pore volumes are 0.03–0.93 cm^3/g, and the average pore diameter values are in the range of 0.61–5.24 nm [19,21,26,27,40]. The surface area, pore size, and pore volume values of the foams produced within the scope of the study were found to be compatible with the literature.

3.2.5. XRD analysis

Figs. 8–10 showed the x-ray diffraction patterns used to determine the crystalline structures (amorphous, crystalline, or semi-crystalline) of carbon foams. The hexagonal carbon, orthorhombic graphite, and hexagonal graphite structures were represented by the peaks located at specific 2θ values in XRD patterns [19]. The characteristic peaks in x-ray diffraction patterns of carbon foams were defined by crosschecking with the JCPDS (Joint Committee on Powder Diffraction Standards) card numbers 98-061-7290, 98-002-9123, 98-008-8811/8812, 98-005-3781. The (0 0 2) and (1 0 0) peaks of the randomly stacked graphene sheets aligned to the peaks seen at 2θ = 23° and 43° in the diffraction patterns of carbon foams [18,21,26,41]. These peaks can be seen in the XRD patterns of bio-based carbon foams produced from birch [21] and larch [26] sawdusts that have been solvolytically liquefied, as well as mesoporous carbon membranes developed by pyrolyzing combinations of poly(furfuryl alcohol) and poly(ethylene glycol) [42]. Due to the absence of diffraction peaks at 23° and 31° (0 0 2) in the XRD patterns, it was concluded that the *HRF* resin foams had amorphous structures (Fig. 8). The resin foams diffraction patterns lacked any sign of a (1 0 0) peak, implying that they did not exhibit a crystalline structure. According to the XRD patterns in Fig. 8, peak formation was observed for *HRFT-3* around 25.03°, 32.45°, 34.11°, 40.90°, and 54.33°, and for *HRFT-5* at 25.03°, 32.45°, 37.19°, and 54.49° in the resin foams structure produced by adding tar as a solvent. It was determined that a peak formation was noticed in the diffraction patterns of the carbon foams prepared as a result of carbonizing or activating the resin foams, thus the crystalline structure started to

Table 4
Structural properties of carbon foams produced by solvolytic liquefaction of *HS*.

S/B ratio	Foam code	S_{BET} (m^2/g)	V_{total} (cm^3/g)	V_{micro} (cm^3/g)	V_{meso} (cm^3/g)	D_{av} (nm)
3/1	*HCF-3*	467.492	0.2657	0.1520	0.1137	2.27
	HCFT-3	243.231	0.1593	0.0720	0.0873	2.62
	HCFA-3	977.35	0.44757	0.31373	0.13384	2.07
	HCFTA-3	1454.39	0.62308	0.47388	0.14920	2.05
5/1	*HCF-5*	472.130	0.2404	0.1670	0.0734	2.04
	HCFT-5	310.48	0.1671	0.0730	0.0941	2.76
	HCFA-5	719.50	0.38329	0.23209	0.15120	2.51
	HCFTA-5	925.50	0.39798	0.28808	0.10990	2.03

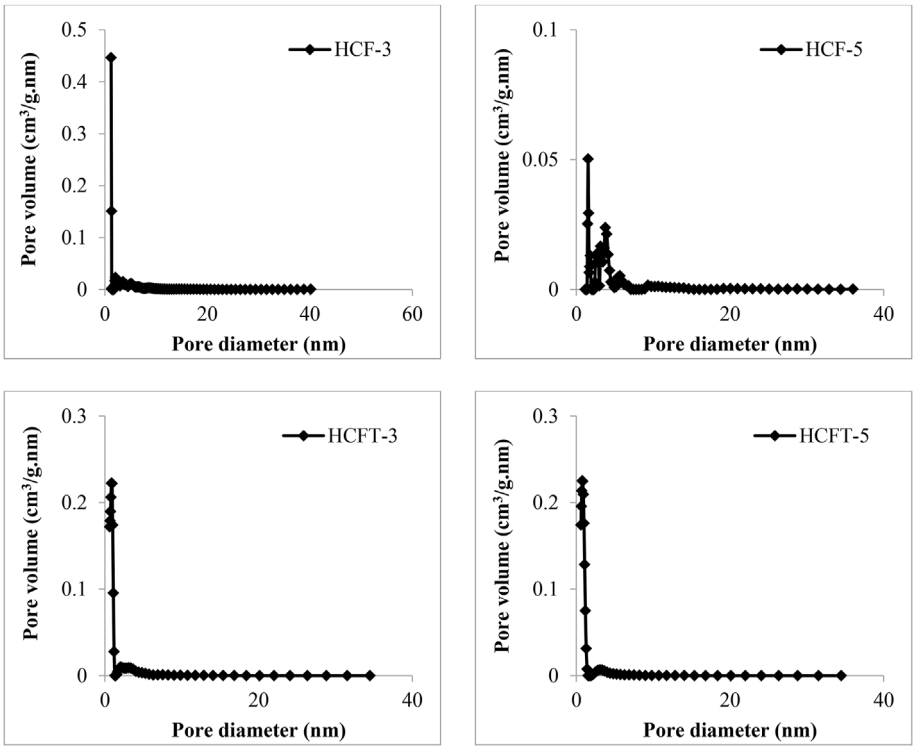

Fig. 6. Pore size distribution curves of carbon foams (effect of solvent type and ratio).

form (Figs. 9 and 10). When only phenol is used as a solvent, the presence of orthorhombic graphite, hexagonal graphite, and hexagonal carbon at 25°, hexagonal carbon around 47° and orthorhombic graphite at 54° in the structure of the carbon foam formed with solvent/biomass ratio = 3/1 (*HCF-3*) were detected. In addition, peaks indicating orthorhombic graphite structure in the carbon foams of *HCF-3* and *HCF-5* were observed in the range of 30–37° for both solvent/biomass ratios (Fig. 9). As shown in Fig. 9, orthorhombic graphite structure was identified in the range of 30–37°, followed by hexagonal graphite and hexagonal carbon at around 25°, and then orthorhombic graphite at 40° and 54° for the carbonized foams (*HCFT-3* and *HCFT-5*). Fig. 10 displayed the X-ray diffraction patterns of activated carbon foams produced after resin foams were chemically activated with potassium hydroxide by varying the solvent/biomass weight ratios and solvent type. The presence of orthorhombic graphite, hexagonal graphite, and hexagonal carbon at about 25°, orthorhombic graphite in the range of 30–37°, hexagonal carbon at around 47°, and orthorhombic graphite at 54° were appointed in the structure of activated carbon foams.

Evaluating the d_{002} values listed in Table 5, it was found that the d_{002} values obtained near 23° ranged between 0.3767 and 0.4003 nm. These data exceeded the value of 0.3350 nm [43,44] attributed to graphite and indicated the non-graphitized carbon structure [21]. It can be concluded that the structure was more irregular when the solvent ratio was raised since there was an increase in the d_{002} value obtained at 23° when the phenol/biomass weight ratio was 5/1 in carbon foams made by employing just phenol.

The carbon foams (0 0 2) diffraction patterns include amorphous (A), turbostratic (T), and graphitic (G) carbon components. "A-component" is the term used to describe the typical broad peak found in irregular carbon-based materials. One distinct, significant diffraction peak can be seen in the (0 0 2) reflection for the "T-component" at about 26.0. This leads to an interlayer spacing along the c-axis of 0.343 nm, which is slightly greater than h-graphite (0.335 nm). A further intense (0 0 2) reflection identified about 26.5–26.6 known as the "G-component", indicating h-graphite with a narrower interlayer spacing (0.335 nm). The presence of the "G-component" indicates heterogeneous, catalytic graphitization. The chemical activation stage reduced defects and enhanced the carbon matrixs hierarchical order. Additional "graphitic-like" areas formed as the chemical activation involved (as shown in the TEM images), and the position of the (0 0 2) reflection shifted slightly

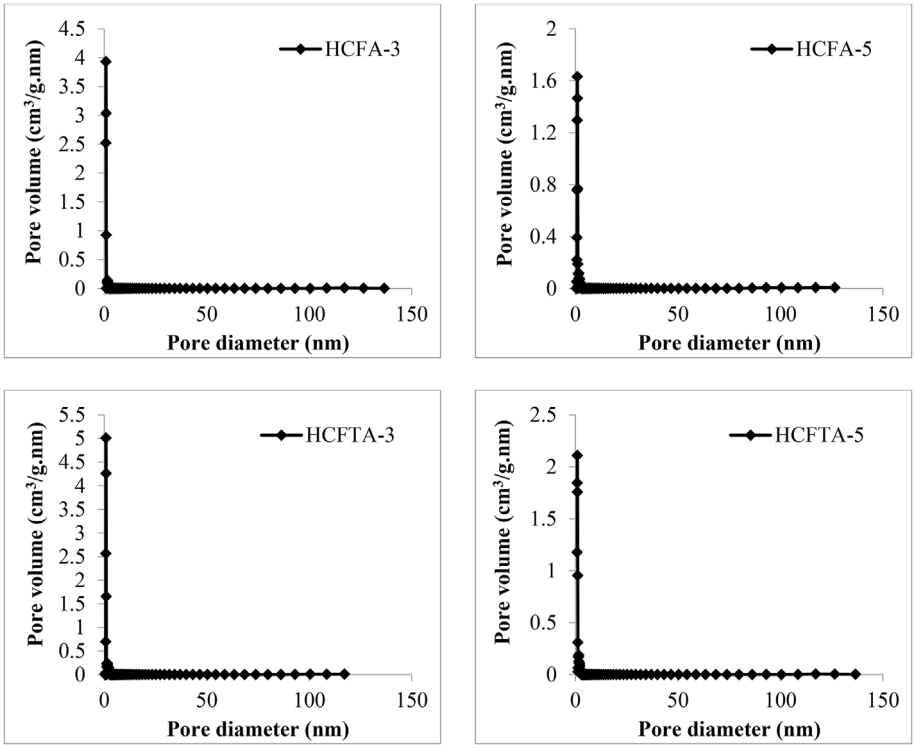

Fig. 7. Pore size distribution curves of carbon foams (effect of chemical activation).

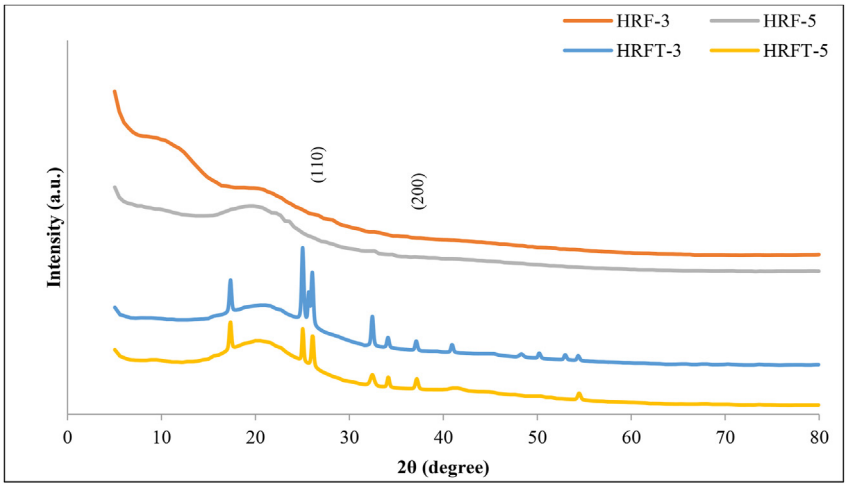

Fig. 8. XRD patterns of resin foams (effect of solvent type and ratio).

closer to that suggested by "G-component". The graphitization impact of the chemical activation agent at a low temperature of 800 °C can be expressed by the relative amount of "G-component" [45]. It was revealed that the sharp peak at about 26° in the diffraction pattern of activated carbon foams was identified as being caused by graphite and had an interplanar spacing of ~0.339 nm [46]. The studies on the impact of coal heat treatment on the carbon structure [26] and the clarification of the crystal structures of biomass-based granular activated carbons have taken into account the d_{002} value, which expresses the gap value between the aromatic graphene layers. In x-ray diffraction patterns, the (0 0 2) peak, defined as the characteristic peak for carbonaceous materials, is usually detected at elevated temperatures (around 1400–1500 °C) for materials with similar chemical structure, such as eucalyptus lignin and rigid phenol-formaldehyde resin-based fibers. The identification of this peak at the lower carbonization temperature applied in the study was related to the facilitation of the development of carbon crystals due to the structural alignment at the beginning of the heating process due to the existence of low molar weight molecules in the structure. In graphite-like materials, the peaks of (1 0 0) and (1 0 1) at $2\theta = 41–45°$ are typical reflections of the two-dimensional configuration of carbon layers [47].

3.2.6. Scanning and transmission electron microscopy image analyses

SEM images required to investigate the morphological structures of resin (*HRF-3*, *HRFT-3*, *HRF-5*, and *HRFT-5*) and carbon foams (*HCF-3*, *HCFT-3*, *HCF-5*, and *HCFT-5*) obtained by polymerization

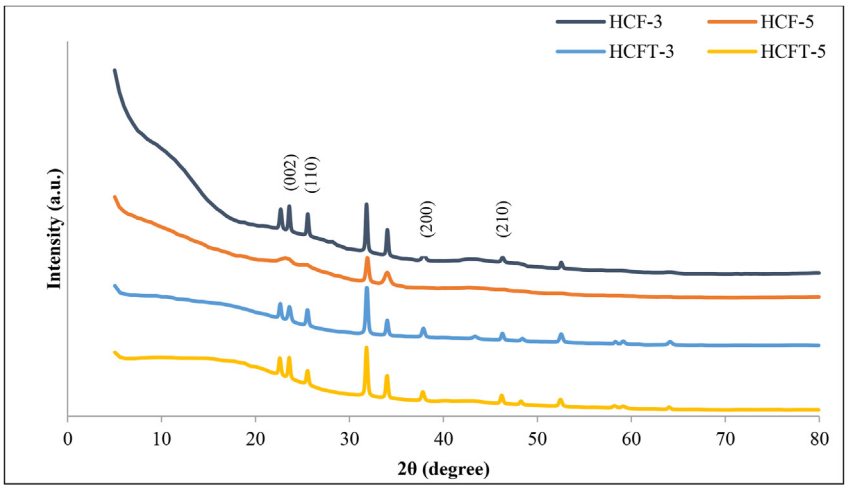

Fig. 9. XRD patterns of carbon foams (effect of solvent type and ratio).

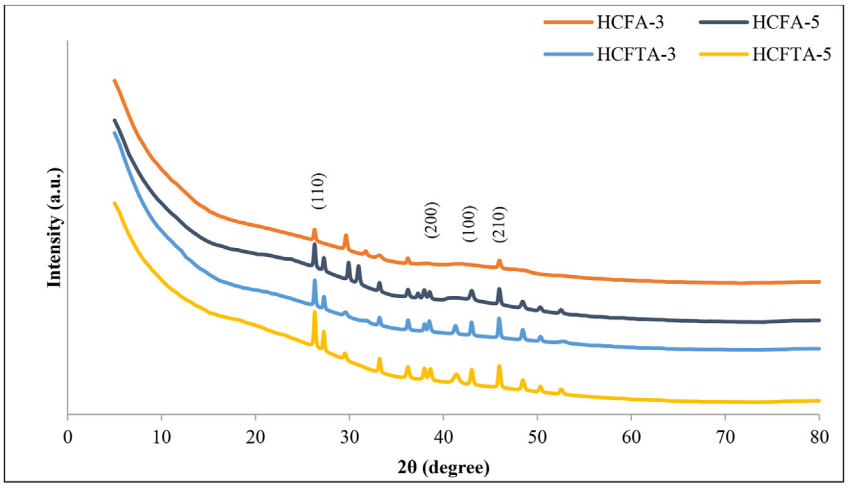

Fig. 10. XRD patterns of activated carbon foams (effect of chemical activation).

Table 5
XRD parameters of carbon foams.

S/B ratio	Foam code	2θ (002) (°)	d_{002} (nm)	2θ (100) (°)	d_{100} (nm)
3/1	*HCF-3*	23.60	0.3767	43.03	0.2100
	HCFT-3	22.66	0.3921	46.28	0.1960
	HCFA-3	26.29	0.3387	45.96	0.1973
	HCFTA-3	26.31	0.3385	45.93	0.1974
5/1	*HCF-5*	22.19	0.4003	–	–
	HCFT-5	22.56	0.3921	46.20	0.1963
	HCFA-5	26.30	0.3386	45.94	0.1974
	HCFTA-5	26.31	0.3385	45.96	0.1973

and foaming processes after conventional and alternative solvolytic liquefaction methods are shown in Figs. 11 and 12. It was revealed that the honeycomb-like cavities created in the foams framework contained errant varying pentagonal and hexagonal patterns (Fig. 11a and b, Fig. 12a and b). Carbon foams had considerably smaller cell sizes and more regular cell structures than resin foams because carbonization yielded the resin foam to become narrow. However, it is reported that when resin foams were heated to the carbonization temperature, certain covered cells were opened by fracturing the layers and the thin layers between the cells evolved thinner and more conspicuous [21]. According to the SEM images of the carbon foams produced with a solvent mixture of phenol and tar, closed pores were developed in the resin foams structural arrangement (Fig. 11c and d), and the pores were opened by changing the structure as a result of the carbonization process (Fig. 12c and d). The SEM images showed that the carbon foams produced without the usage of tar had an open pore structure (Fig. 12a and b), while the phenol/biomass ratio was 5/1, the prepared foams were more regular and had fewer cell cracks. Carbon foams voids and cell sizes vary between 30 and 100 μm for the S/B = 3/1 ratio and 100–400 μm for the S/B = 5/1 ratio (Fig. 12a and b). In the majority of the cell morphologies of the produced foams, adjacent cells, ligaments, and node development were seen. There were numerous microscopic pores in the cells aforementioned regions, ranging in size from 2 to 5 μm, which could be the result of the foaming agents smaller cores (Fig. 12a and b). When tar was incorporated into the synthesis mixture, more heterogeneous and irregular cell morphologies as well as rigid foams with more closed pore structures were formed, in contrast to the structures of carbon foams produced without employing tar. This observation can be explained through the hypothesis that the complex components of tars structure prevent to move away the foaming agents introduced to the synthesis mixture, which must be eliminated from the

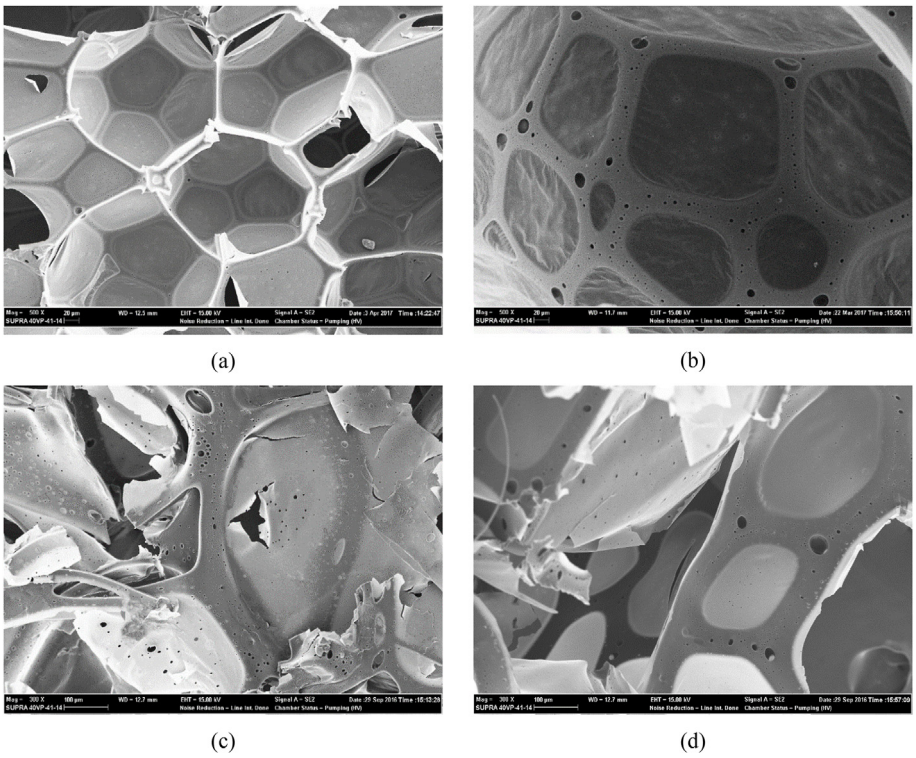

Fig. 11. SEM images of resin foams (a) *HRF-3*, (b) *HRF-5*, (c) *HRFT-3*, and (d) *HRFT-5*.

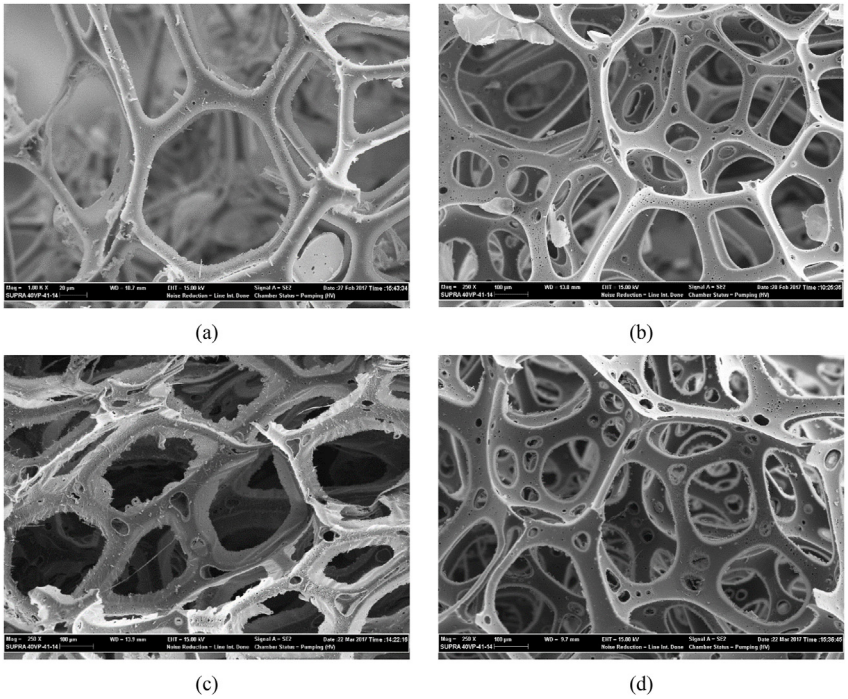

Fig. 12. SEM images of carbon foams (a) *HCF-3*, (b) *HCF-5*, (c) *HCFT-3*, and (d) *HCFT-5* (effect of solvent type and ratio).

polymer matrix throughout the reaction. The prior geometries of the resin foams were retained after the activation process because of their thermoset structure. When tar was added as a solvent, it was noticed that the voids and cell sizes of the carbon foams were in the range of 50–250 μm, smaller pores of 5–20 μm were composed at the ligament and nodes of the pores, the size of the openings altered inversely with the amount of solvent incorporated, and the foaming degree reduced as the solvent proportion raised (Fig. 12c and d). Fig. 13 displayed SEM images of carbon foam and potassium hydroxide-activated carbon foams intended for sorption operations that were acquired at a magnification of 1000×. It was obvious that additional pores were developing in the

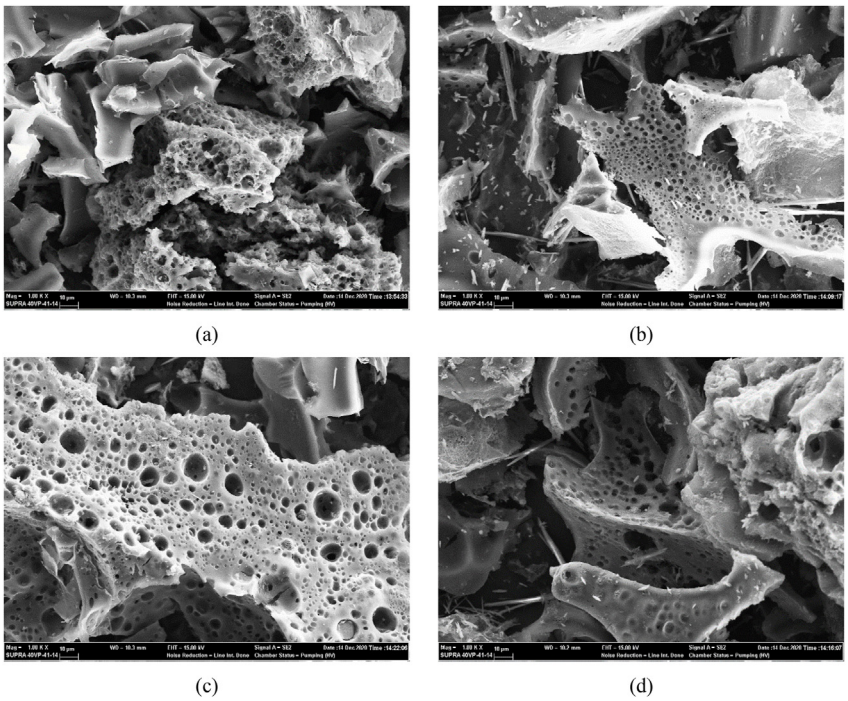

Fig. 13. SEM images of carbon foams (a) *HCFA-3*, (b) *HCFTA-3*, (c) *HCFA-5*, and (d) *HCFTA-5* (effect of chemical activation).

foams morphologies after the chemical activation step. The activated-foam structure contained pores with diameters ranging from 1 to 10 μm. Although uniform cells existed in several foam morphologies, some structures had fractures and some cell walls were damaged after a chemical activation procedure. It is confirmed in the literature that when moisture and foaming ingredients are released from resin foam frameworks during carbonization and activation, the foam structures shatter. Finally, it was noticed that the carbon foams exhibited an amorphous porous structure relying on the TEM images (Figs. 14 and 15) evaluated to determine the textural features. Another remarkable feature in the TEM images consistent with SEM and XRD analyses was the darker coloration of the graphitic carbon regions generated by the overlap of graphene layers. This occurs as a result of greater electron scattering in certain regions including few-layer graphene sheets. It is notable that when the chemical activation was implemented, the typical peak (0 0 2) for graphite also arises in the XRD pattern at around 26.3°, which could be attributable to the conversion of some of the bio-polyol-based amorphous carbon to crystalline graphite.

3.2.7. Compressive strength measurement and porosity calculation

It is known that compressive strength, which is the characteristic mechanical property of carbon foams, is related to the density and surface area of the foam. Contemplating that the bulk densities of carbon foams synthesized from different wood types in the literature were approximately 0.02 g/cm^3 [21,26,27], in this study, the bulk densities (0.0248 and 0.0194 g/cm^3 as seen in Fig. 16) of hornbeam sawdust-based carbon foams synthesized using the traditional solvolytic liquefaction method using different solvent/biomass weight ratios seem to conform with the studies in the literature. As the quantity of added solvent was raised, the bulk and true densities of carbon foams were reduced. In contrast, it was revealed that the polymeric structure of the tar introduced as a solvent to the synthesis mixture elevated the true and bulk densities of the carbon foams. Wood-based carbon foams with ultra-high porosity above 92% were formed by solvolytically liquefied hornbeam sawdust. As a side effect of the micro- and meso-pores in the structure of foam determined by nitrogen adsorption/desorption analysis, the bulk density, the strength of the cross-linking in the polymer matrix, and the material resistance all decrease [21,27,48–50]. Recognizedly, the compressive strengths of denser carbon foams are significantly higher. Also, it has been reported that the structures weak cell walls and large cell size diminish compressive strength as proven by SEM analysis [51]. In our earlier study [19], a thorough review of the literature on the interaction between the density and compressive strength of carbon foams prepared from different precursors was conducted. The compressive strengths of carbon foams produced by solvolytic liquefaction of hornbeam sawdust, which was presumed to be comparable to the compressive strengths of conventional phenolic foams (0.025–0.620 MPa) despite being relatively weak than carbon foams derived from fossil fuels [27,52], were varied between 0.229 and 0.333 MPa (Fig. 16). In summary, it was concluded that compared to foams formed by using the conventional method, carbon foams with enhanced strength could be created when both the type and quantity of the solvent were varied.

3.2.8. Raman spectra analysis

The crystal structure and electrical characteristics of carbon-based materials are investigated using Raman spectroscopy. This technique can be applied to examine D (diamond-like), G (graphite-like), and 2D bands as well as the number of graphenes layers, quality of layers, defects in its structure, regular and irregular structures, and doping level. Significant Raman bands of carbon-based materials such as graphene are called the G and 2D bands. Changes in temperature and chemical doping can affect these bands. As the number of graphene layers varies, the shape, position, and intensity of the G and 2D bands alter. On the other hand, the D-band offers details regarding the level of defect and irregularity in the crystal structure of graphene, including edge defects and heteroatom contribution [53]. The D band, which signifies the defects

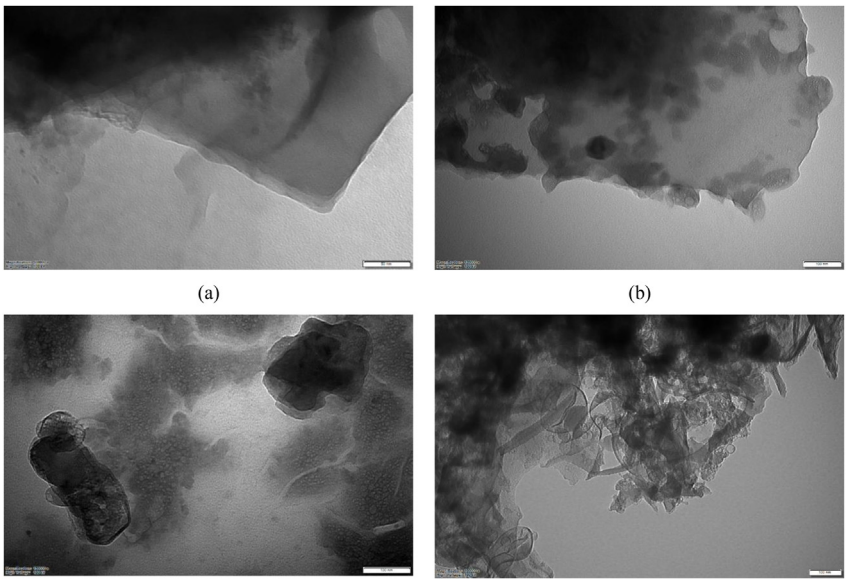

Fig. 14. TEM images of carbon foams for solvent/biomass weight ratio of 3/1; (a) *HCF-3*, (b) *HCFA*-3, (c) *HCFT-3*, and (d) *HCFTA-3*.

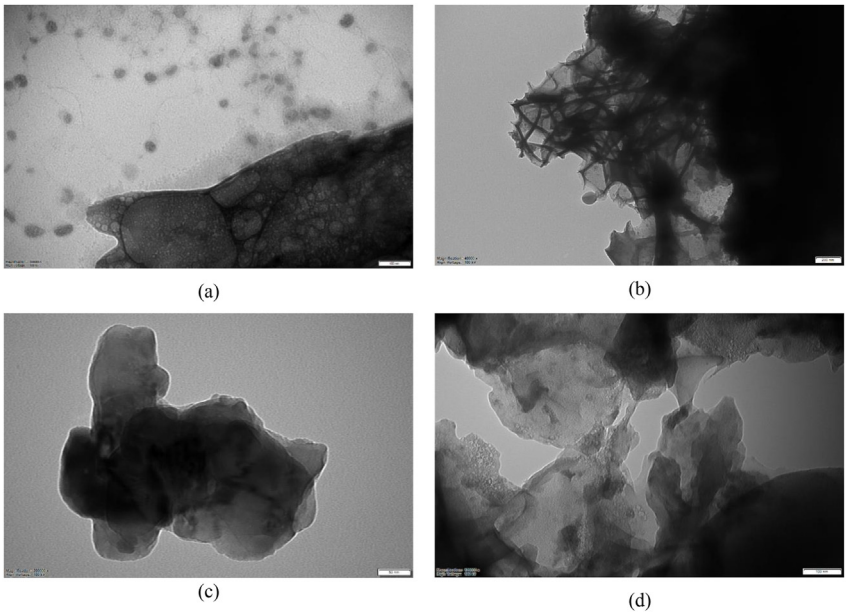

Fig. 15. TEM images of carbon foams for solvent/biomass weight ratio of 5/1; (a) *HCF-5*, (b) *HCFA-5*, (c) *HCFT-5*, and (d) *HCFTA-5*.

in the structure and provides the C—C bond stretching vibrations (sp^3 vibrations) in the graphene structure, was seen at about 1345 cm^{-1}, as determined by Raman spectra of the carbon foams (Fig. 17). Additionally, the graphene peak, a narrower G band arising from C=C bond in-plane stretch vibrations (sp^2 vibrations), was located at around 1600 cm^{-1} [20,53]. Accordingly, it was deduced that *HCFTA-3*, the carbon foam with the lowest D band intensity, had a higher graphitization degree than the other foams [20,54].

3.3. Investigation of CO_2 adsorption capacities of carbon foams

Fig. 18 illustrated the isotherms of the analyses performed at 0 °C to investigate the ability of carbon foams to adsorb CO_2 as a pollutant gas. By evaluating all measured data, the maximum CO_2 adsorption capacity of 6.53 mmol/g was recorded for *HCFA-3* carbon foam that was produced with a solvent/biomass weight ratio of 3/1 and activated with KOH. Consistent with the surface areas of the carbon foams, the CO_2 sorption capacity of the foams produced by the activation procedure was assessed to be 19—75% higher than the samples without the activation process. Zhang et al. [55] formed hierarchically porous multi-walled carbon nanotubes/carbon foam (MCF) nanocomposites utilizing liquefied larch sawdust as a raw material, and 2% by weight of MWCNT added nanocomposite (MCF-2) exhibited good CO_2 adsorption capacities such as 4.58 and 3.19 mmol/g at 0 and 25 °C, respectively. In a different study, Zhang et al. [56] produced graphene oxide/carbon foam (GCF) nanocomposites from larch sawdust that had been liquefied. When they added 0.2% by weight of graphene oxide, it was found

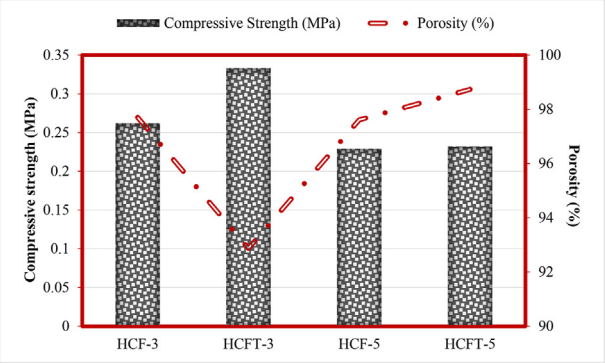

Fig. 16. Carbon foams association between compressive strength and porosity.

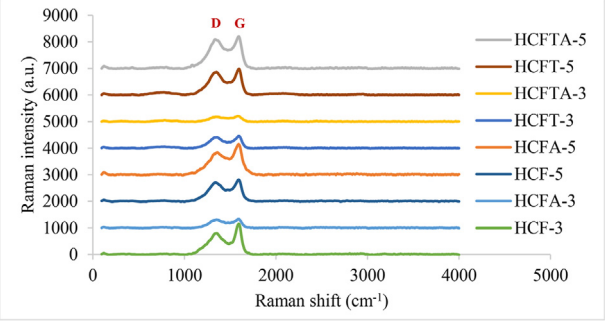

Fig. 17. Raman spectra of carbon foams.

that the resulting GCF-0.2 material had the highest CO_2 capacity, measuring 4.99 mmol/g at 0 °C and 1 bar. Rodríguez and García [57] prepared hierarchical coal-based carbon foams utilizing $ZnCl_2$ and KOH as activating agents, and they reported that the CO_2 holding capacity of carbon foam activated with $ZnCl_2$ was between 1.6 and 2.1 mmol/g while that of carbon foam activated with KOH was up to 2.8 mmol/g. In their study, Narasimman et al. [58] obtained 3.37 mmol/g CO_2 adsorption capacity in open cellular carbon foams produced from molten sucrose employing an aluminum nitrate blowing agent. As a consequence, the 6.53 mmol/g capacity had shown to be more efficient than the others when the CO_2 adsorption capacities of the biomass-based carbon foams in the literature were compared with those of the hornbeam sawdust-based carbon foams prepared in this work.

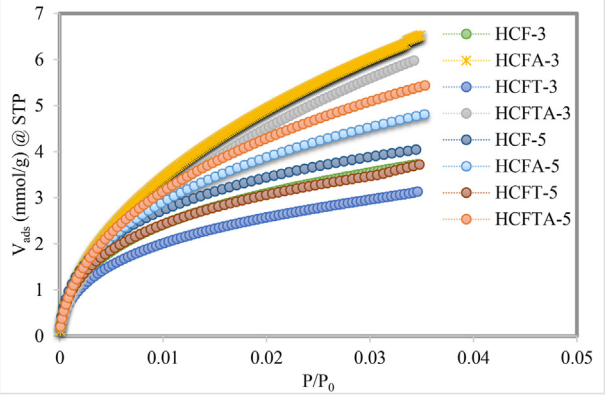

Fig. 18. CO_2 adsorption isotherms of carbon foams.

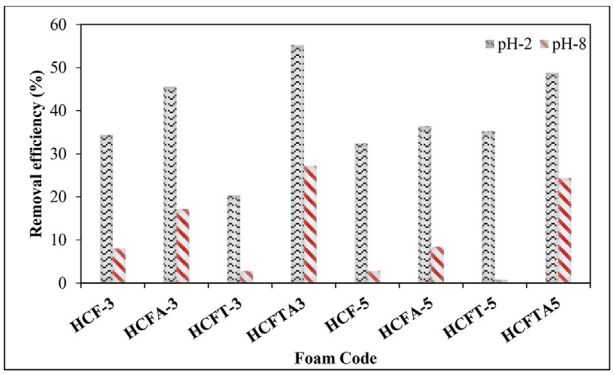

Fig. 19. Dye removal efficiencies (%) of carbon foams.

3.4. Investigation of dye adsorption capacities of carbon foams and statistical modeling

Adsorption tests were performed to assess the effectiveness of hornbeam sawdust-based carbon foams in removing dye from aqueous solutions using 25 ppm Pr Navy Hexl dye. The influences of incorporating tar as a solvent in the solvolytic liquefaction process, solvent/biomass weight ratio, alkaline activation technique using potassium hydroxide, and aqueous solution acidity on the color removal efficiency (%) were evaluated. The chemical activation process raised the uptake level of dye, as shown by the adsorption experiment results in Fig. 19. Reactive dyes are known to be adsorbed more effectively at low pH values. It was ascertained that the adsorbing ability of carbon foams improved with the increase of effective adsorption areas because of the larger surface area after the chemical activation process. The carbon foam with the code *HCFTA-3*, which involved adding tar as a solvent in the liquefaction process and applying chemical activation to the resin foams, was found to have the maximum removal performance (55.2%) when the pH of the *NH* dye solution was 2.

Dye removal efficiency (η, %) values were used as the dependent variable (response) in statistical analysis achieved with the assistance of MINITAB 17 software. The testing conditions to be investigated in the adsorption process were defined with the two-level full factorial experimental design; main and interaction effects plots were evaluated as well as normal probability plots of standard effects and Pareto charts. Additionally, analysis of variance at a 95% confidence level was used to assess the interactions between the independent variables and the most significant factors [24,59]. The linear equation shown in Eq. (3) represented the relationship

Table 6
Statistical parameters for 2^4 full factorial experimental design in *NH* dye removal.

Term	Effect	Coef	T-value	*P*-value
Constant		25.00	23.85	0.027
A	−2.70	−1.35	−1.29	0.421
B	3.70	1.85	1.76	0.329
C	15.80	7.90	7.52	0.084
D	−27.10	−13.55	−12.90	0.049
*A*B*	3.60	1.80	1.71	0.336
*A*C*	−4.10	−2.05	−1.95	0.301
*A*D*	−2.00	−1.00	−0.95	0.516
*B*C*	8.30	4.15	3.95	0.158
*B*D*	1.00	0.50	0.48	0.717
*C*D*	−0.10	−0.05	−0.05	0.970
*A*B*C*	−1.40	−0.70	−0.67	0.626
*A*B*D*	−1.30	−0.65	−0.62	0.647
*A*C*D*	3.00	1.50	1.43	0.389
*B*C*D*	0.00	0.00	0.00	1.000

Table 7
Results of the variance analysis (ANOVA).

Source	*DF*	*Adj SS*	*Adj MS*	*F-ratio*	*P-value*
Model	14	4485.40	320.39	18.16	0.182
Linear	4	4020.12	1005.03	56.97	0.099
A	1	29.16	29.16	1.65	0.421
B	1	54.75	54.76	3.10	0.329
C	1	998.56	998.56	56.61	0.084
D	1	2937.64	2937.64	166.53	0.049
2-way interaction	6	414.68	69.11	3.92	0.369
*A*B*	1	51.84	51.84	2.94	0.336
*A*C*	1	67.24	67.24	3.81	0.301
*A*D*	1	16.00	16.00	0.91	0.516
*B*C*	1	275.56	275.56	15.62	0.158
*B*D*	1	4.00	4.00	0.23	0.717
*C*D*	1	0.04	0.04	0.00	0.970
3-way interaction	4	50.60	12.65	0.72	0.697
*A*B*C*	1	7.84	7.84	0.44	0.626
*A*B*D*	1	6.76	6.76	0.38	0.647
*A*C*D*	1	36.00	36.00	2.04	0.389
*B*C*D*	1	0.00	0.00	0.00	1.000
R^2 (%)	99.61				

between the experimental variables and the corresponding response. The coefficients from the statistical analysis were substituted into the equation, and the effect of the related sorbent on the dye removal efficiency (%) was derived.

$$Y = X_0 + X_1A + X_2B + X_3C + X_4D + X_5AB + X_6AC + X_7AD + X_8BC + X_9BD + X_{10}CD + X_{11}ABC + X_{12}ABD + X_{13}ACD + X_{14}BCD \quad (3)$$

where X_0 is the constant coefficient, X_i is the coefficient relevant to the effects and interactions of the main factors, and Y is the predicted response (dye removal efficiency,%). The variables solvent/biomass weight ratio, tar contribution, chemical activation, and pH are denoted by the letters *A*, *B*, *C*, and *D*, respectively. Analysis of variance was applied to accomplish the statistical analysis of the variables and to investigate the interaction effects in the removal of *NH* dye from an aqueous medium. Tables 6 and 7 displayed the

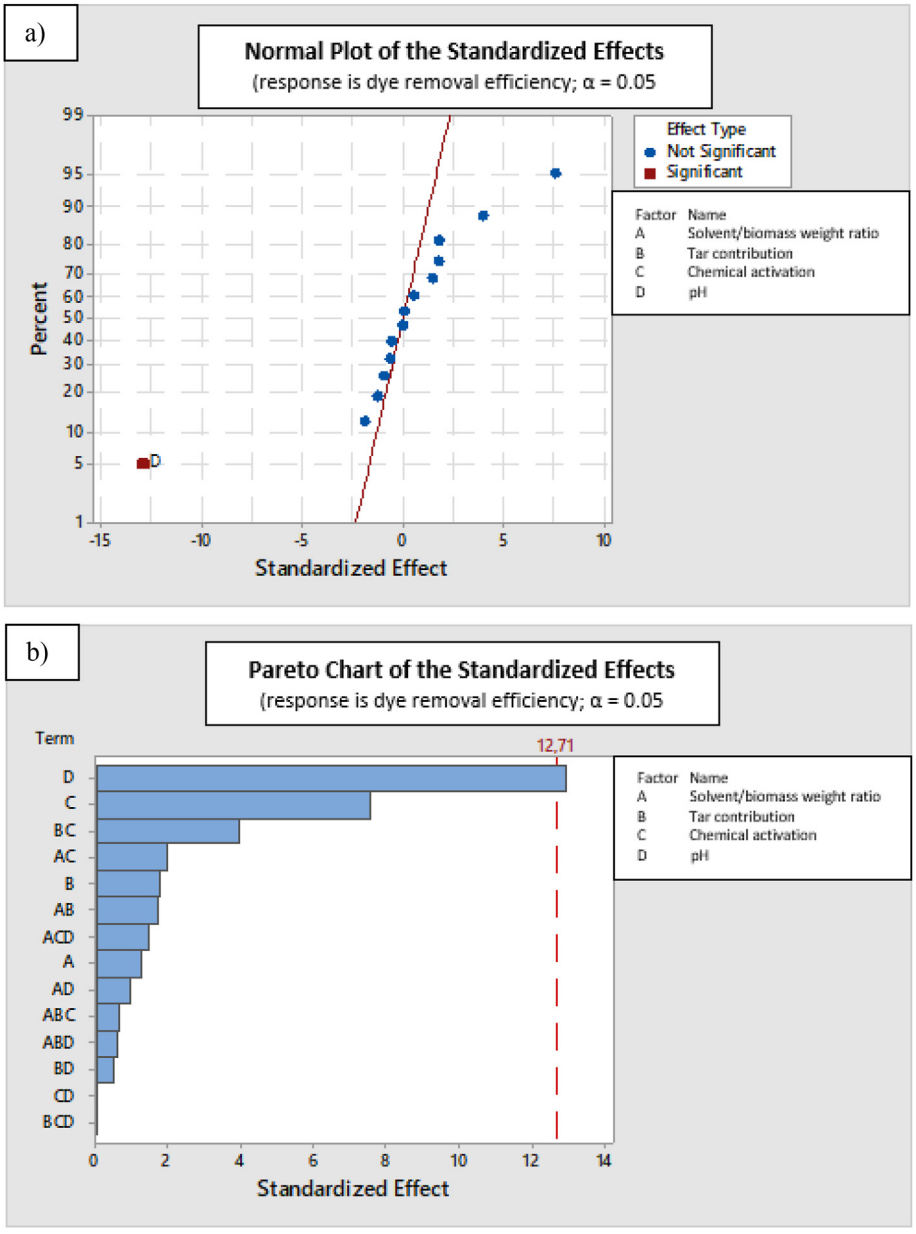

Fig. 20. (a) Normal probability of the standardized effects and (b) Pareto chart for *NH* dye removal efficiency (%).

main and interaction effects, probability values (*P*-value), Students-T-test values, and Fisher F-ratios determined by the analysis.

The main effect of solution pH was assessed to be highly significant with a significance level of $P < 0.05$ due to the results of the variance analysis. Furthermore, the model was projected to be appropriate for hornbeam sawdust-based carbon foam sorbents. The experimental values for carbon foams applied as adsorbents were found to be in agreement with the values derived from the statistical model, according to the evaluation of the correlation coefficient ($R^2 = 99.61$) value of the relevant model. Eq. (3) was rearranged using the X_i coefficients acquired as a result of variance analysis, and Eq. (4) provided the model equation with all coefficients for *NH* dye removal efficiency (%). When analyzing the effect of a factor, positive coefficients are acquired if the response value (removal efficiency, %) obtained when operating under high-level conditions instead of low-level conditions also increases, and negative coefficients are attained if the response value decreases. For instance, the terms *A*, *D*, *A*C*, *A*D*, *C*D*, *A*B*C*, and *A*B*D* exhibit negative coefficients when hornbeam sawdust-based carbon foams were utilized as sorbents. Accordingly, for every 1% increase in solution pH, *NH* dye removal efficiency was reduced by 13.55% while all other factors remain constant.

$$\eta\,(\%) = 25.00 - 1.35\,A + 1.85\,B + 7.90\,C - 13.55\,D + 1.80\,A{*}B - 2.05\,A{*}C - 1.00\,A{*}D + 4.15\,B{*}C + 0.50\,B{*}D - 0.05\,C{*}D - 0.70\,A{*}B{*}C - 0.65\,A{*}B{*}D + 1.50\,A{*}C{*}D + 0.00\,B{*}C{*}D \quad (4)$$

Each effect is represented by a point on a normal probability plot, and the distribution of the main and interaction effects are evaluated. Standardized effects are t-statistics confirming the null hypothesis that the effect is "0". The normal probability plot of the standardized effects for *NH* dye sorption was given in Fig. 20a. When the distribution of the normal probability plot was inspected, it was clear that all of the points for the dye adsorption via carbon

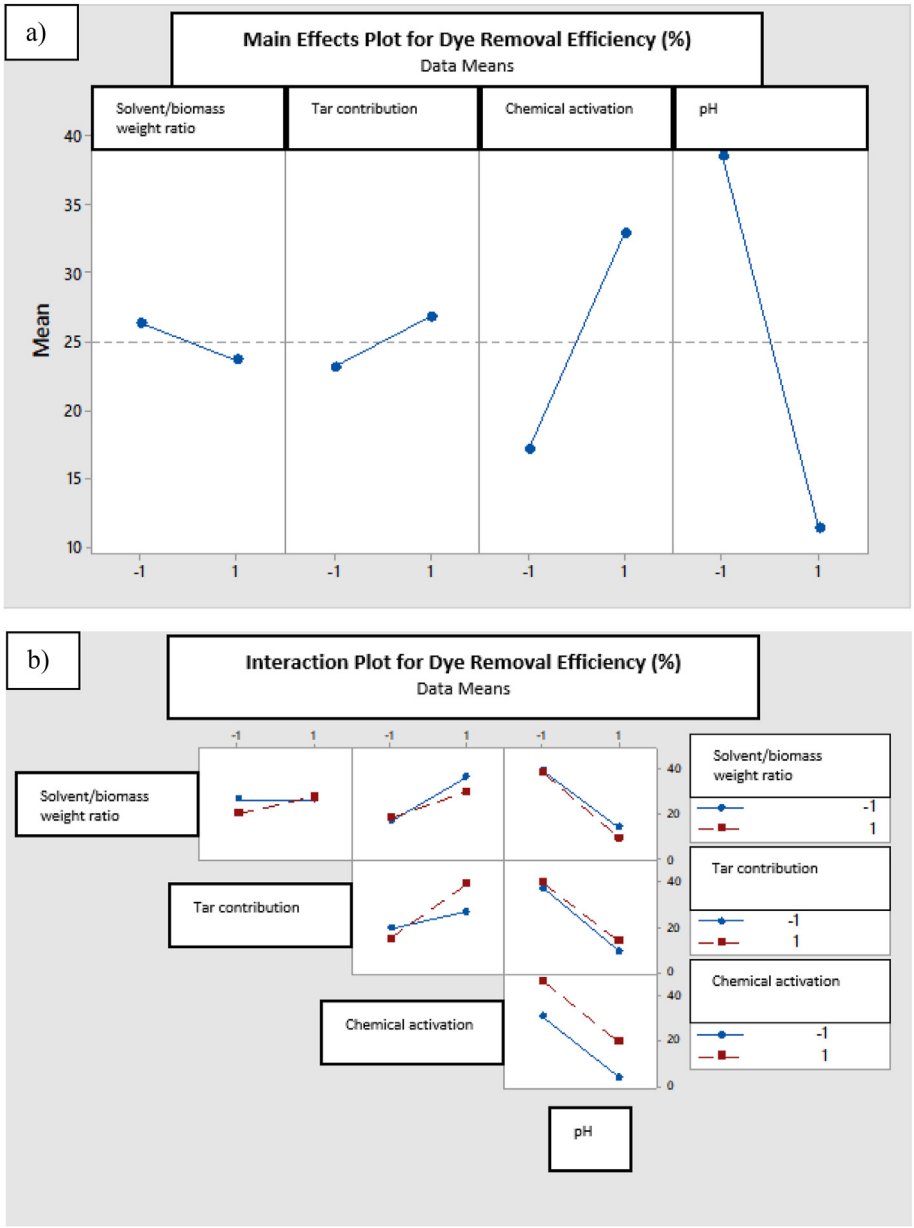

Fig. 21. Plots of (a) the main effects and (b) the interaction effects for *NH* dye removal efficiency (%).

foam fell between −15 and +10. Positive coefficients are specified for the factors on the right side of the normal probability plots, and negative coefficients are defined for the factors on the left side. Information regarding the significance of each main effect and their interaction effects was provided by the Pareto chart of the standardized effects in Fig. 20b. The normal distribution plot, a graphical tool used to evaluate whether a data set is nearly uniformly distributed or not, was compatible with the Pareto chart, and the effects on the right side of the red striped line (the pH effect for this study) in the Pareto chart were regarded as significant. According to the Pareto chart, three effects with the most significant impact could be ranked as *pH> Chemical activation > Tar contribution*Chemical activation* (*D > C > B*C*).

When evaluating the factor effects, it is reported that the level depends on whether the response (dye removal efficiency, %) changes when the level is altered and can have either a positive or negative value. When the main effects of *NH* dye removal were examined (Fig. 21a), it was noticed that pH and the solvent/biomass weight ratio (*A* and *D*) had negative effects. The height of the line connecting two levels is intrinsically linked with the statistical degree of change caused by the effect during the level variation. For instance, a significant decline in dye removal efficiency was detected when the pH of the solution was raised. On the other hand, it was revealed that the tar contribution and chemical activation had a favorable impact on the response (dye removal efficiency, %). It is crucial to examine both the main effects and the interaction effects while implementing statistical analysis. Non-parallel lines are detected when the interaction effect between the two factors is highly considerable. The graphs of the binary interaction effects of the four factors that were influential in eliminating dye from aqueous solutions with carbon foam were provided in Fig. 20b. Hence, it was determined that the interactions between pH and each main effect (*solvent/biomass weight ratio*pH*, *tar contribution*pH*, *chemical activation*pH*; symbolized as *A*D*, *B*D*, and *C*D*) were more prominent than other interactions.

4. Conclusions

The development of carbon foam from bio-polyols prepared via the liquefaction method by evaluating alternative renewable raw material sources supports the concept of circular economy as well as provides waste management and sustainable development. It was confirmed by this study that bio-polyol-based carbon foam was successfully prepared from solvolytic liquefaction of hornbeam tree sawdust, resinification, and foaming stages. GC/MS, ^{1}H NMR, and FT-IR analyses indicated that the bio-polyol was a hydroxyl-rich source that was suitable for synthesizing carbon foam. The chemical structure of bio-polyols had a remarkable effect on the foaming process. The pyrolysis tar of hornbeam sawdust was primarily assessed as a solvent in the production of carbon foam. The impacts of two solvent types (phenol and tar-mixed-phenol), various solvent/biomass weight ratios (3/1 and 5/1 w/w) during solvolytic liquefaction method and chemical activation of the resin foam with potassium hydroxide on the mechanical and physical characteristics of carbon foams were inspected in this context. The surface area of the carbon foam, which was produced without using tar, with a solvent/biomass ratio of 3/1 and activated with KOH, increased by 109%. The elemental composition, morphological structure, and crystallographic characteristics of carbon foams were considerably influenced by the chemical activation procedure, in addition to the quantity and kind of solvent utilized in the liquefaction process. When the CO_2 uptake performances were examined, it was determined that *HCFA-3* carbon foam activated with KOH had the highest capacity with 6.53 mmol/g. When the dye adsorbing capacities of carbon foams from aqueous solutions were compared, dye adsorption was noticeably improved due to the enhanced porosity with the chemical activation procedure. Foam-coded *HCFTA-3*, which was successful in the CO_2 uptake process, adsorbed 55.2% dye uptake with a surface area of 1454.9 m^2/g. In conclusion, considering the potential of organic wastes to be cost-effective and abundant sources for the synthesis of polyol compounds, this study reported that it is possible to utilize renewable and waste materials for the production of bio-polyol-based carbon foams, one of the advanced carbonaceous materials.

CRediT authorship contribution statement

Adife Seyda Yargic: Conceptualization, Methodology, Formal Analysis, Investigation, Writing-Review&Editing. **Gamze Gunduz Meric:** Formal Analysis, Writing-Original Draft. **Rahmiye Zerrin YARBAY:** Writing-Original Draft. **Nurgul OZBAY:** Supervision.

Declaration of competing interest

The authors declare that they have no known competing financial interests or personal relationships that could have appeared to influence the work reported in this paper.

Data availability

No data was used for the research described in the article.

Acknowledgments

The authors would like to thank the Bilecik Seyh Edebali University Scientific Research Projects Coordination Unit under the Grant Numbers 2018−01. BŞEÜ.03-10 and 2020−01. BŞEÜ.03-08 for financial support.

References

[1] H. Bai, N. Liu, L. Hao, P. He, C. Ma, R. Niu, J. Gong, T. Tang, Self-floating efficient solar steam generators constructed using super-hydrophilic N, O dual-doped carbon foams from waste polyester, Energy Environ. Mater. 5 (4) (2022) 1204−1213.
[2] S. Wu, D. Chen, G. Zhao, Y. Cheng, B. Sun, X. Yan, W. Han, G. Chen, X. Zhang, Controllable synthesis of a robust sucrose-derived bio-carbon foam with 3D hierarchical porous structure for thermal insulation, flame retardancy and oil absorption, Chem. Eng. J. 434 (2022) 134514.
[3] Ö. Bağ, K. Tekin, Production and characterization of hydrothermal carbon from waste lignocellulosic biomass, J. Fac. Eng. Archit. Gazi Univ. 35 (2) (2019) 1063−1076.
[4] Y. Shi, X. Xia, J. Li, J. Wang, T. Zhao, H. Yang, J. Jiang, X. Jiang, Solvolysis kinetics of three components of biomass using polyhydric alcohols as solvents, Bioresour. Technol. 221 (2016) 102−110.
[5] N. Haleem, A. Khattak, Y. Jamal, M. Sajid, Z. Shahzad, H. Raza, Development of polyvinyl alcohol (PVA) based biochar nano fibers for carbon dioxide (CO2) adsorption, Renewable Sustainable Energy Rev. 157 (2022) 112019.
[6] C. He, H. Wang, L. Fu, J. Huo, Z. Zheng, C. Zhao, M. An, Principles for designing CO2 adsorption catalyst: serving thermal conductivity as the determinant for reactivity, Chin. Chem. Lett. 33 (2) (2022) 990−994.
[7] S. Wang, Y.R. Lee, Y. Won, H. Kim, S.E. Jeong, B.W. Hwang, A.R. Cho, J.Y. Kim, Y.C. Park, H. Nam, D.H. Lee, H. Kim, S.H. Jo, Development of high-performance adsorbent using KOH-impregnated rice husk-based activated carbon for indoor CO2 adsorption, Chem. Eng. J. 437 (2022) 135378.
[8] Z. Qiang, R. Li, Z. Yang, M. Guo, F. Cheng, M. Zhang, Zeolite X adsorbent with high stability synthesized from bauxite tailings for cyclic adsorption of CO2, Energy Fuels 33 (7) (2019) 6641−6649.
[9] L.B. Sun, Y.H. Kang, Y.Q. Shi, Y. Jiang, X.Q. Liu, Highly selective capture of the gren house gas CO2 in polymers, ACS Sustain. Chem. Eng. 3 (12) (2015) 3077−3085.
[10] A.Z. Peng, S.C. Qi, X. Liu, D.M. Xue, S.S. Peng, G.X. Yu, X.Q. Liu, L.B. Sun, Fabrication of N-doped porous carbons for enhanced CO2 capture: rational design of an ammoniated polymer precursor, Chem. Eng. J. 369 (2019) 170−179.
[11] S. Liu, L. Rao, P. Yang, X. Wang, L. Wang, R. Ma, L. Yue, X. Hu, Superior CO2 uptake on nitrogen doped carbonaceous adsorbents from commercial phenolic resin, J. Environ. Sci. 93 (2020) 109−116.

[12] C. Ma, T. Lu, J. Shao, J. Huang, X. Hu, L. Wang, Biomass derived nitrogen and sulfur co-doped porous carbons for efficient CO2 adsorption, Sep. Purif. Technol. 281 (2022) 119899.
[13] M. Priyanka, M.P. Saravanakumar, Ultra high adsorption capacity of starch derived zinc based carbon foam for adsorption of toxic dyes and its preliminary investigation on oil-water separation, J. Clean. Prod. 197 (2018) 511–524.
[14] X. Zhang, K. Wang, C. He, Y. Lin, H. Hu, Q. Huang, H. Yu, T. Zhou, Q. Lin, Regulation pore size distribution for facilitating malachite green removal on carbon foam, Environ. Res. 213 (2022) 113715.
[15] Y. Zhang, Q. Wang, R. Li, Z. Lou, Y. Li, A novel phenolic foam-derived magnetic carbon foam treated as adsorbent for rhodamine B: characterization and adsorption kinetics, Crystals 10 (3) (2020) 159.
[16] H. Li, T. Li, W. Deng, S. Kong, Preparation and adsorption properties of graphene-modified, pitch-based carbon foam composites, Polymers 14 (20) (2022) 44–55.
[17] X. Lu, Z. Li, Y.A. Liu, B. Tang, Y. Zhu, J.M. Razal, E. Pakdel, J. Wang, X. Wang, Titanium dioxide coated carbon foam as micro reactor for improved sunlight driven treatment of cotton dyeing wastewater, J. Clean. Prod. 246 (2020) 118949.
[18] A.Ş. Yargıç, R.Z.Y. Şahin, N. Özbay, Investigation of solvent type effect on the structural properties of bio-polyol-based carbon foam, J. Fac. Eng. Archit. Gazi Univ. 36 (1) (2021) 133–145.
[19] N. Ozbay, A.S. Yargic, Carbon foam production from bio-based polyols of liquefied spruce tree sawdust: effects of biomass/solvent mass ratio and pyrolytic oil addition, J. Appl. Polym. Sci. 136 (11) (2019) 47185.
[20] A.S. Yargic, N. Ozbay, Effect of chemical activation on the cellular structure of biopitch-derived green carbon foam, Diam. Relat. Mater. 96 (2019) 58–66.
[21] R. Wang, W. Li, S. Liu, A porous carbon foam prepared from liquefied birch sawdust, J. Mater. Sci. (2012) 1977–1984.
[22] F. Ning, W. Cong, Y. Hu, H. Wang, Additive manufacturing of carbon fiber-reinforced plastic composites using fused deposition modeling: effects of process parameters on tensile properties, J. Compos. Mater. 51 (4) (2017) 451–462.
[23] M. Riera-Torres, M.C. Gutiérrez, Colour removal of three reactive dyes by UV light exposure after electro chemical treatment, Chem. Eng. J. 156 (1) (2010) 114–120.
[24] A. Yargic, A.S. Yargic, N. Ozbay, Utilization of factorial design methodology to optimize Pr Red Hegxl dye uptake and prediction of removal efficiency via artificial neural network: comparison of linear vs non-linear sorption isotherm and kinetic parameters, Biomass Convers. Biorefin. 13 (3) (2023) 1723–1750.
[25] J.H. Harker, J.R. Backhurst, Fuel and Energy, Academic Press Limited, London, 1981.
[26] W. Li, Z. Huang, Y. Wu, X. Zhao, S. Liu, Honeycomb carbon foams with tunable pore structures prepared from liquefied larch sawdust by self foaming, Ind. Crops Prod. 64 (2015) 215–223.
[27] A.S. Yargic, Ordered reticulated-structured carbon foams via surfactant-addition into the polymerization medium of bio-based polyols, Chem. Eng. Process: Process Intensif. 158 (2020) 108204.
[28] K.A. Trick, T.E. Saliba, Mechanisms of the pyrolysis of phenolic resin in a carbon/phenolic composite, Carbon 33 (11) (1995) 1509–1515.
[29] I. Allen, V.E. Meharg, J.H. Schmidt, Chemistry of synthetic varnish resins, Ind. Eng. Chem. 26 (6) (1934) 663–669.
[30] J.I. Ozaki, W. Ohizumi, A. Oya, A TG-MS study of poly (vinyl butyral)/phenol-formaldehyde resin blend fiber, Carbon 10 (38) (2000) 1515–1519.
[31] H. Jiang, J. Wang, S. Wu, Z. Yuan, Z. Hu, R. Wu, Q. Liu, The pyrolysis mechanism of phenol formaldehyde resin, Polym. Degrad. Stabil. 97 (8) (2012) 1527–1533.
[32] G.P. Shulman, H.W. Lochte, Thermal degradation of polymers. II. Mass spectrometric thermal analysis of phenol-formaldehyde polycondensates, J. Appl. Polym. Sci. 10 (4) (1966) 619–635.
[33] S.I. Talabi, A.P.D. Luz, V.C. Pandolfelli, V.H. Lima, V.R. Botaro, A.D.A. Lucas, Graphitization of lignin-phenol-formaldehyde resins, Mater. Res. 23 (2) (2020) e20190686.
[34] R.C.S. Araújo, V.M.D. Pasa, Mechanical and thermal properties of polyurethane elastomers based on hydroxyl-terminated polybutadiene sand biopitch, J. Appl. Polym. Sci. 88 (3) (2003) 759–766.
[35] R. Araújo, V. Pasa, New eucalyptus tar-derived polyurethane coatings, Prog. Org. Coating 51 (2004) 6–14.
[36] B. Melo, V. Pasa, Composites based on eucalyptus tar pitch/castor oil polyurethane and shortsisal fibers, J. Appl. Polym. Sci. 89 (14) (2003) 3797–3802.
[37] R. Araújo, V. Pasa, B. Melo, Effects of biopitch on the properties of flexible polyurethane foams, Eur. Polym. J. 41 (6) (2005) 1420–1428.
[38] K.S. Sing, R.T. Williams, Physisorption hysteresis loops and the characterization of nanoporous materials, Adsorpt. Sci. Technol. 22 (10) (2004) 773–782.
[39] P.T. Williams, A.R. Reed, Development of activated carbon pore structure via physical and chemical activation of biomass fibre waste, Biomass Bioenergy 30 (2) (2006) 144–152.
[40] S. Liu, Z. Huang, R. Wang, A carbon foam with a bimodal micro–mesoporous structure prepared from larch sawdust for the gas-phase toluene adsorption, Mater. Res. Bull. (2013) 2437–2441.
[41] M.S. Strano, A.L. Zydney, H. Barth, G. Wooler, H. Agarwal, H.C. Foley, Ultrafiltration membrane synthesis by nanoscale templating of porous carbon, J. Membr. Sci. 198 (2) (2002) 173–186.
[42] M.S. Strano, H. Agarwal, J. Pedrick, D. Redman, H.C. Foley, Templated pyrolytic carbon: the effect of poly (ethyleneglycol) molecular weight on the pore size distribution of poly (furfurylalcohol)-derived carbon, Carbon 41 (13) (2003) 2501–2508.
[43] R. Bansode, J. Losso, W. Marshall, R. Rao, R. Portier, Adsorption of volatile organic compounds by pecan shell- and almond shell-based granular activated carbons, Bioresour. Technol. 90 (2) (2003) 175–184.
[44] H. Takagi, K. Maruyama, N. Yoshizawa, Y. Yamada, Y. Sato, XRD analysis of carbon stacking structure in coal during heat treatment, Fuel 83 (17–18) (2004) 2427–2433.
[45] A. Kotronia, H.D. Asfaw, C.W. Tai, K. Edström, D. Brandell, Catalytically graphitized freestanding carbon foams for 3D Li-ion microbatteries, J. Power Sources Adv. 1 (2020) 100002.
[46] C.H. Manoratne, S.R. Rosa, I.R. Kottegoda, XRD-HTA, UV Visible, FTIR and SEM Interpretation of Reduced Graphene Oxide Synthesized from High Purity Vein Graphite, Mat. Sci. Res. India, 2017, pp. 19–30.
[47] M.J. Prauchner, V.M. Pasa, N.D. Molhallem, C. Otani, S. Otani, L.C. Pardini, Structural evolution of Eucalyptus tar pitch-based carbons during carbonization, Biomass Bioenergy 28 (1) (2005) 53–61.
[48] C. Chen, E.B. Kennel, A.H. Stiller, P.G. Stansberry, J.W. Zondlo, Carbon foam derived from various precursors, Carbon 44 (8) (2006) 1535–1543.
[49] S.M. Manocha, K. Patel, L.M. Manocha, Development of carbon foam from phenolic resin via template route, Indian J. Eng. Mater. Sci. 17 (2010) 338–342.
[50] N. Ozbay, A.S. Yargic, Liquefaction of oak tree bark with different biomass/phenol mass ratios and utilizing bio-based polyols for carbon foam production, AIP Publishing LLC In AIP Conference Proceedings 1809 (1) (2017) 020039.
[51] A.A. Septevani, D.A. Evans, C. Chaleat, D.J. Martin, P.K. Annamalai, A systematic study substituting polyetherpolyol with palm kernel oil based polyester polyol in rigid polyurethane foam, Ind. Crops Prod. 66 (2015) 16–26.
[52] C.G. Dos-Santos, M.A. Costa, W.A. De Morais, V.M. Pasa, Phenolic foams from wood tar resols, J. Appl. Polym. Sci. 115 (2) (2010) 923–927.
[53] E. Kılıç, Preparation and Characterization of Graphene-Based Green Nanocomposites and Their Utilization in Various Applications, Graduate School of Science and Engineering, Department of Chemistry, Doktoral Thesis, Ankara, 2019. Hacettepe University.
[54] S. Li, Y. Tian, Y. Zhong, X. Yan, Y. Song, Q. Guo, L. Liu, Formation mechanism of carbon foams derived from mesophase pitch, Carbon (2011) 618–624.
[55] Y. Zhang, J. Sun, J. Tan, C. Ma, S. Luo, W. Li, S. Liu, Multi-walled carbon nanotubes/carbon foam nanocomposites derived from biomass for CO_2 capture and supercapacitor applications, Fuel 305 (2021) 121622.
[56] Y. Zhang, J. Sun, J. Tan, C. Ma, S. Luo, W. Li, S. Liu, Hierarchical porous graphene oxide/carbon foam nanocomposites derived from larch for enhanced CO_2 capture and energy storage performance, J. CO_2 Util. 52 (2021) 101666.
[57] E. Rodríguez, R. García, Low-cost hierarchical micro/macroporous carbon foams as efficient sorbents for CO_2 capture, Fuel Process. Technol. 156 (2017) 235–245.
[58] R. Narasimman, S. Vijayan, K. Prabhakaran, Carbon foam with microporous cell wall and strut for CO_2 capture, RSC Adv. 4 (2) (2014) 578–582.
[59] N. Ozbay, A.S. Yargic, Statistical analysis of Cu (II) and Co (II) sorption by apple pulp carbon using factorial design approach, J. Ind. Eng. Chem. 57 (2018) 275–283.